

This is a repository copy of *Artificial neural network based photovoltaic fault detection algorithm integrating two bi-directional input parameters*.

White Rose Research Online URL for this paper:

<https://eprints.whiterose.ac.uk/177732/>

Version: Accepted Version

---

**Article:**

Hussain, Muhammad, Dhimish, Mahmoud, Titarenko, Sofya et al. (1 more author) (2020) Artificial neural network based photovoltaic fault detection algorithm integrating two bi-directional input parameters. *Renewable Energy*. pp. 1272-1292. ISSN 0960-1481

<https://doi.org/10.1016/j.renene.2020.04.023>

---

**Reuse**

This article is distributed under the terms of the Creative Commons Attribution-NonCommercial-NoDerivs (CC BY-NC-ND) licence. This licence only allows you to download this work and share it with others as long as you credit the authors, but you can't change the article in any way or use it commercially. More information and the full terms of the licence here: <https://creativecommons.org/licenses/>

**Takedown**

If you consider content in White Rose Research Online to be in breach of UK law, please notify us by emailing [eprints@whiterose.ac.uk](mailto:eprints@whiterose.ac.uk) including the URL of the record and the reason for the withdrawal request.

# Artificial Neural Network based photovoltaic fault detection algorithm integrating two bi-directional input parameters

*Muhammed Hussain, Mahmoud Dhimish, Sofya Titarenko, Peter Mather*

*University of Huddersfield, Laboratory of Photovoltaics, Huddersfield, HD1 3DH, United Kingdom*

**Abstract**— In this paper, a fault detection algorithm for photovoltaic systems based on artificial neural networks (ANN) is proposed. Numerous literatures can be found on the topic of PV fault detection through the implementation of artificial intelligence. The novel part of this research is the successful development, deployment and validation of a fault detection PV system using radial basis function (RBF), requiring only two parameters as the input to the ANN (solar irradiance and output power). The results obtained through the testing of the developed ANN on a PV installation of 2.2 kW capacity, provided an accuracy of 97.9%. To endorse the accuracy of the newly developed algorithm, the ANN was tested on another PV system, installed at a remote location. The total capacity of the new system was significantly higher, 4.16 kW. A vital part of the test was to see how the proposed ANN would perform with ‘scaled-up’ input data, during normal operation as well as partial shading scenarios. The validation process provided an overall fault detection accuracy of above 97%. The decrease in accuracy was due to the varying nature of the two systems in terms of total capacity, number of samples and type of faults.

**Keywords**—Photovoltaics; Fault Detection; Artificial Intelligence; RBF Network.

## 1. Introduction

### 1.1 Research Background

Technological advancements in both hardware and software have enhanced the monitoring and analysis of grid-connected photovoltaic (GCPV) systems, for optimal energy harvesting along with reliable power production. The increase in the installation of PV due to its numerous benefits, means researchers are actively looking into the development of diagnostic methods for fault detection in PV plants.

PV systems process monitoring is based on a distributed sensor network (DSN), for analysis of the system and performance reviews. Corresponding time series analysis of obtained data is vital for statistical analysis of PV systems. The implementation of fault detection in PV systems can become complex depending on the variety of data being logged. A DSN may consist of several variables such as current, voltage, irradiance and temperature [1-2]. Therefore, the complexity of the process may hinder enterprises from implementing fault detection in their systems.

33 Researchers have proposed numerous methods to ease the complexity of failure detection systems  
34 by decreasing the number of input variables required, along with more sophisticated statistical  
35 analysis [3-4]. This paper proposes the use of Artificial Neural Networks (ANN) for this purpose.

36 Various fault detection techniques for PV systems are widely available in the literature, with  
37 varying accuracy levels, detection speed and algorithm complexity. Prediction of faults in PV  
38 systems through the utilisation of metrological and satellite data is one of the techniques used [5-  
39 6]. Whilst other fault detection algorithms for PV systems do not require any climate data [7].

40 Fault detection in PV systems can be split into three categories visual, thermal and electrical [8].  
41 Before looking deeper into the electrical category, it is important to mention another technique  
42 which is also applicable, known as Electro Luminescence Imaging (EL). This technique is based  
43 on the solar module being supplied with external excitation current through its metal contacts,  
44 acting as a light emitting diode. A sensitive Si-CCDs camera can then take an image of the emitted  
45 photons at a wavelength greater than 850nm.

46 The electrical category is further divided into sub-categories consisting off:

- 47 • Methods that do not require any climate data (solar irradiance, temperature). An example  
48 of this approach is the Time-Domain Reflectometry (TDR) proposed in [9] for detection  
49 of disconnection of a PV string.
- 50 • Methods based around the analysis of the current and voltage characteristics. S. Silvestre  
51 *et al.* [10] calculates Series Resistance ( $R_s$ ), Fill Factor (FF) and Shunt Resistance ( $R_{sh}$ )  
52 based on the I-V characteristics leading on to performance indicators. Fault detection for  
53 PV systems based on the evaluation of current and voltage indicators.
- 54 • Methods based around Maximum Power Point Tracking (MPPT). X. Li *et al.* [11] Proposes  
55 an automatic supervision and fault detection method based on power loss analysis. The  
56 approach led to the identification of faults including faulty module, faulty string and faults  
57 linked to partial shading, MPPT failure and ageing.
- 58 • Methods based on Artificial Intelligence (AI) techniques. Authors' in [12] look at the  
59 effectiveness of BP neural network for fault diagnosis in PV systems, comparing it to Fuzzy  
60 Logic. The author concludes BP neural network as the solution to most limitation faced  
61 through the implementation of Fuzzy Logic in fault detection of PV systems.

62 Artificial neural networks (ANNs) are mathematical tools, imitating biological human neural  
63 networks, learning from experience and generalizing previous behaviour as characteristics [13].  
64 The ANN architecture consists of an input layer, one or more hidden layers and an output layer.  
65 ANN's ability to process information in non-linear, high-parallelism, fault and noise environments  
66 makes it of considerable interests to researchers in many fields [14-16]. In comparison to  
67 traditional model-based methods, ANN's are data-driven, self-adaptive methods learning from  
68 examples whilst picking-up subtle and hidden functional relationships that are otherwise unknown  
69 or hard to describe. In addition, ANNs are suitable for solving problems where explicit knowledge  
70 is difficult to identify, but a vast amount of data is available [17-19]. A. Lapedes *et al.* [20],

71 demonstrates how backpropagation neural networks surpass by order of magnitude any of the  
72 conventional linear and polynomial methods dealing with chaotic time series of data. In addition,  
73 A. Millit *et al.* [21] demonstrates ANN networks as a solution for the modelling and estimating of  
74 output power for PV systems. Whereas, F. Polo *et al.* [22] proposes a failure mode prediction and  
75 energy harvesting of PV systems to support dynamic maintenance tasks using ANN-based models.  
76 Ultimately, it looks to analyse data and disregard the erroneous prediction of faults in a PV system.  
77 The paper implements a back-propagation network, trained on historical data consisting of past  
78 five years of an inverter used in the PV system. Highlighting the nature of failures under  
79 consideration, the paper describes the faults as a result of equipment deterioration and useful life  
80 reduction owing to operational and geographical features. The author in his conclusion claims that  
81 the proposed methodology could further improve its performance if ‘enough data’ is available for  
82 significant training of the ANN.

83 Yasuhiro Yagi *et al.* [23] proposes a learning method based on expert systems for the identification  
84 of two types of faults (shading effect and inverters failure). The main advantage of this technique  
85 is that it relies on simple and reprogrammable ANN network, but, on the other hand, the proposed  
86 technique cannot identify faulty conditions occurring in PV systems such as PV short circuit failure  
87 conditions and PV String failure. An advanced ANN network proposed by [24] demonstrates the  
88 detection of faults in the DC part of a PV system such as faulty bypass diodes, faulty PV modules,  
89 and faulty PV string. The paper proposes two algorithms based on MLP and RBF networks. The  
90 confusion matrix shows the accuracy of the MLP (90.3%) was higher than that of RBF (68.4%).  
91 It is a well-known fact that MLP networks, have a much higher accuracy as compared to RBF and  
92 are more commonly used. Especially in networks requiring more hidden layers. However, it is also  
93 important to note that MLP networks are more demanding in terms of computational time.  
94 Therefore, if the use of multiple hidden layers is not required, then an RBF network can be  
95 implemented saving computational time and appealing to a broader audience. However, the data  
96 set consists of a modest number of samples (775). Also, the data set does not consist of real-time  
97 data from a PV-system, but rather it is simulated using MATLAB/Simulink. Conversely, the data  
98 sample used in our proposal consists of 97200 samples over a 10-week, obtained from a live  
99 installation, refer to section 2.

100 Yuchuan Wu *et al.* [25] looks at the limitations of Fuzzy Logic used in early stages of fault  
101 detection in PV systems. It highlights barriers such as the process for obtaining fuzzy rules and  
102 membership function, along with the constancy of fuzzy systems. This method is implemented  
103 using BP neural networks for fault detection in PV systems, resolving the issues faced with Fuzzy  
104 logic through its ability to better self-learning, self-adaptability and non-linearity pattern  
105 recognition.

## 106 **1.2 Contribution and Paper Organization**

107 The main contribution of this work is to present a novel algorithm that can carry out fault detection  
108 in a PV system, to a high degree of accuracy, requiring only two inputs. This is done through the

109 implementation of an RBF network for the classification of the faults presented in section 3.2. The  
110 rationale for the selection of RBF over Multilayer Perceptron Networks (MLP) was due to the  
111 network only requiring a single hidden layer but more importantly due to RBF's robustness to  
112 adversarial samples in the data set. As proven in section 3.1, the ANN architecture accuracy was  
113 compared with a varying number of hidden layers. The results showed that a single hidden layer  
114 was the most optimal solution providing an accuracy of almost 99% while consuming the least  
115 amount of computational time. As a result of this an RBF network was selected rather than an  
116 MLP. Although MLP can also be used in a single hidden layer configuration, it demands more  
117 computational power, further discussed in section 3.8.

118 Rest of the article is organized as follows; Section 2 presents the examined PV installations. In  
119 section 3 we discuss in detail the rationale for selecting RBF over MLP and look at the structure  
120 of the proposed network along with the four different ANN-based methodologies to detect faults  
121 in PV systems. Section 4, looks at the results of the network. In section 5, we compare our  
122 developed ANN network with recent ANN-based models available in present literature. Finally,  
123 sections 6 and 7 present the conclusion and reference list, respectively.

## 124 2. Examined PV system

125 The overall system design is shown in Figure 1. The PV plant consists of 10 PV modules set-up  
126 in string topology, irradiance sensor, MPPT unit and DC- load. The input/output pins of the MPPT  
127 unit are linked via Ethernet-capable to a personal computer (PC) to facilitate real-time data  
128 monitoring. The proposed ANN algorithm for fault detection of the PV modules is developed in  
129 MATLAB software.

130 As shown in Figure 2, the PV plant consisting of 10-polycrystalline silicon PV modules, with a  
131 nominal power of 220 W (per module), the electrical parameters under 'standard test conditions'  
132 (STC) of the PV modules are shown in Table 1; STC of the PV modules at solar irradiance = 1000  
133 W/m<sup>2</sup>, module temperature = 25 °C, spectral distribution of the incident light according to AM 1.5  
134 and irradiation perpendicular onto the receiving plane. The Maximum Power Point Tracker  
135 (MPPT) has an output efficiency of not less than 95.0%. Internal sensors within the MPPT are  
136 used to measure the DC current and voltage.

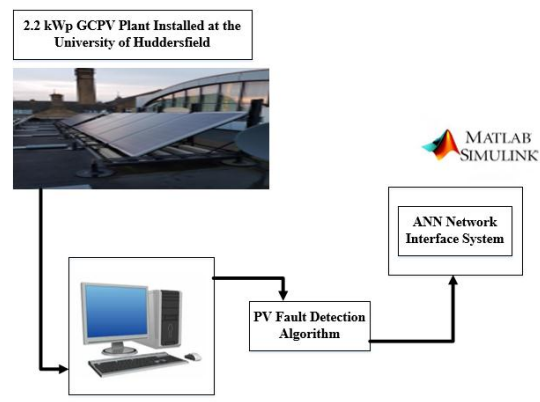


**Figure 1.** Overall System Architecture Design for the Examined PV Plant

**Table 1.** Electrical characteristics of SMT6 (60) P PV module

Solar Panel Electrical Characteristics	Value
Peak Power	220 W
Voltage at maximum power point ( $V_{mpp}$ )	28.7 V
Current at maximum power point ( $I_{mpp}$ )	7.67 A
Open Circuit Voltage ( $V_{oc}$ )	36.74 V
Short Circuit Current ( $I_{sc}$ )	8.24 A
Number of cells connected in series	60
Number of cells connected in parallel	1
Series resistance $R_s$	0.53 $\Omega$
Parallel resistance $R_{sh}$	1890 $\Omega$

137 Davis weather station measures the global solar irradiance, which is passed onto the monitoring  
138 unit connected to the PC for data recording and monitoring. A Hub 4 communication manager  
139 facilitates acquisition of modules temperature via the Davis external temperature sensor, as well  
140 as the electrical data for each photovoltaic string.

141 The weather station is located on the same level and position of the PV modules, as presented in  
142 Figure 2(a). The weather station is mounted near to the examined PV system, the solar irradiance  
143 is measured using a pyranometer which has a resolution of  $\pm 2 \text{ W/m}^2$ , while the angle of incident  
144 is set the same as the PV modules inclination of 37 degrees.

145 If the angle of inclination is changed, therefore, the results of the solar irradiance would typically  
146 impact the ANN detection accuracy, since the solar irradiance against the output predicted power  
147 would be expected to be inaccurate. For generalization purposes, it would be more appropriate to  
148 use a mathematical modeling for the solar irradiance which can predict the output irradiance on a  
149 particular location including the inclination of a typical PV system, this was not the case in our  
150 model, as we ensure that the pyranometer is on the same inclination as the examined PV  
151 installations.

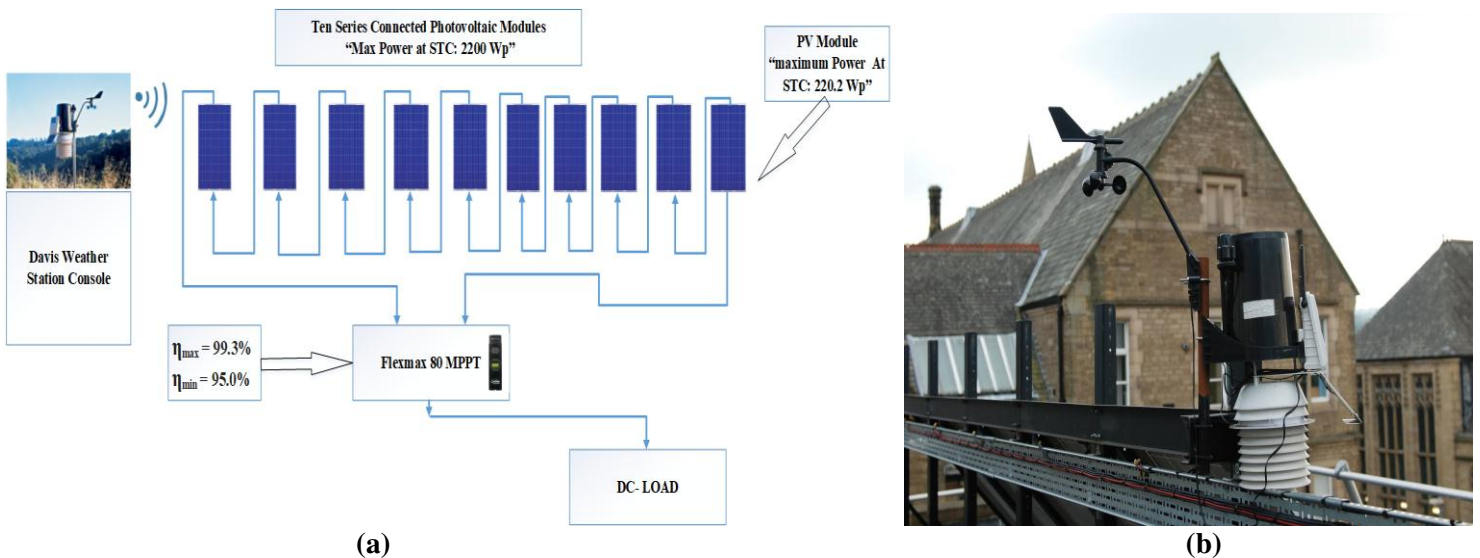


**Figure 2.** (a) Examined PV System layout including the weather station and DC-Load, (b) weather station mounted in the examined PV installation

152 In this article, we have taken a data samples of the PV installation captured over a commencing  
153 period of November 2019 to February 2020. As a result, it might be useful to outline that during  
154 summer period, when the irradiance and ambient temperature is expected to have a high peak, the  
155 prediction and accuracy of any typical ANN network might differ. Hence, in the following section,  
156 we have used four different data input setups to overcome this issue.

### 157 3. Methodology

158 Researchers have demonstrated various methodologies for data normalisation, training, validation  
159 and testing of ANN networks. To the best of our understanding, the majority of the implemented  
160 methodologies found in recent literature are based on data sets, consisting of several inputs to the  
161 network [5, 21 & 24]. The following sub-sections demonstrate in detail the four methodologies  
162 that were implemented on the sample data set consisting of solar irradiance and total output power.  
163 The data consisted of 10 weeks, one week worth of data for every fault, starting with normal  
164 operation (NO). The ANN was trained with each methodology and the overall detection accuracy  
165 for the four methodologies is used as a reference to the success of each.

#### 166 3.1 ANN Structure

167 The purpose of the ANN was to detect faults in PV modules, as shown in Figure 3. Before the  
168 ANN could be trained with a sample data set, the first step was the formation of a strategy, to test  
169 the optimal process for selecting the sample data to train the ANN. For this critical task, four  
170 different methodologies for data processing were investigated:

- 171 1. Methodology 1 (M1): solar irradiance and output power was randomly selected, including  
172 all off-state data (where power is equal to zero), no normalisation process was involved.
- 173 2. Methodology 2 (M2): solar irradiance and output power was randomly selected, all off-  
174 state data was dismissed, no normalisation process was implemented.
- 175 3. Methodology 3 (M3): solar irradiance and output power was randomly selected and  
176 normalised using the max-min normalisation technique.
- 177 4. Methodology 4 (M4): solar irradiance and output power was randomly selected and  
178 normalised. In addition, solar irradiance of 0 - 1000 W/m<sup>2</sup> was mapped along with the  
179 output power.

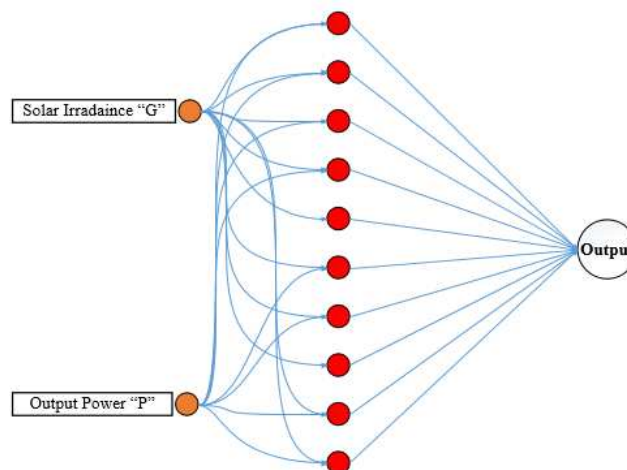


Figure 3. The proposed RBF architecture

180 The architecture of the ANN was based on the Radial Basis Function (RBF). The network was  
 181 made up of three parts (input, hidden layer and output). For this research, a single hidden layer  
 182 was implemented, for all investigative methods, due to the linear nature of the response, high  
 183 accuracy and minimal computational time. The hidden layer can be increased for further accuracy  
 184 and computational performance, depending on the application under consideration. Increasing the  
 185 number of hidden layers would convert the network into an MLP, increasing the computational  
 186 time. The developed ANN architecture using one hidden layer achieved a high rate of detection  
 187 accuracy, almost equal to 99%; this will be discussed in the following sections.

188 In principle, each neuron takes a formed linear combination of the outputs of previous neurons.  
 189 This linear combination is weighted through the strength between the neurons ( $w_{ij}$ ) and multiplied  
 190 by the input ( $x_j$ ). Further, the activation threshold ( $w_{j0}$ ) is also assigned to each neuron. This  
 191 process is expressed using (1). Note:  $i$  is equal to number of hidden neurons (1, 2, 3 ... 10),  $j$  is  
 192 equal to number of inputs (1 and 2).

$$193 \quad \sum_{j=1}^n (w_{ij}x_j + w_{j0}) \quad (1)$$

194 Next, the weighted activation process is then multiplied by the non-linear function  $f_1$  as shown in  
 195 (2), this is usually a sigmoid function (MLP) or Euclidian function (RBF). Finally, the output value  
 196 of the hidden layers  $y_i$  is expressed by (3).

$$197 \quad f_1 \times \sum_{j=1}^n (w_{ij}x_j + w_{j0}) \quad (2)$$

$$198 \quad y_i = f(u) = \frac{1}{1 + e^{-\sum_{j=1}^n (w_{ij}x_j + w_{j0})}} \quad (3)$$

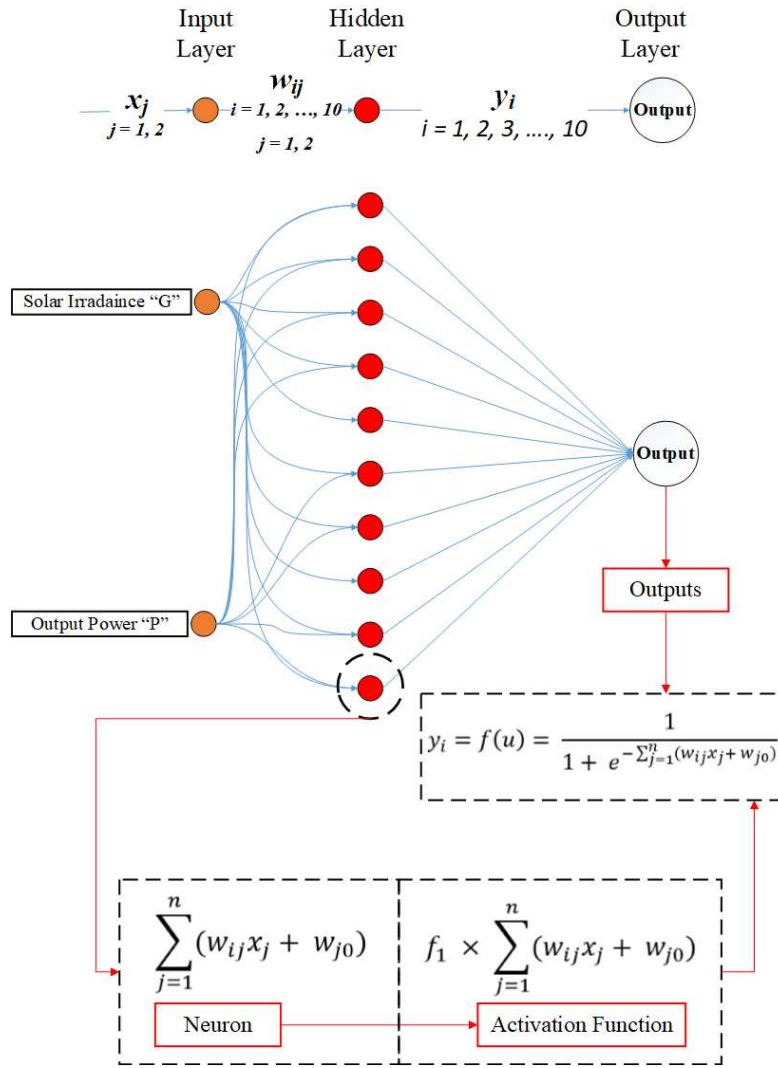
199 in order to enhance the performance of the selected ANN structure, we have used the quick  
 200 prorogation method, expressed by (4), where the tanning iteration number is equal to 1000.

$$201 \quad \Delta w(s) = \frac{\nabla \delta | w(s)}{\nabla \delta | w(s-1) - \nabla \delta | w(s)} \Delta w(s-1) \quad (4)$$

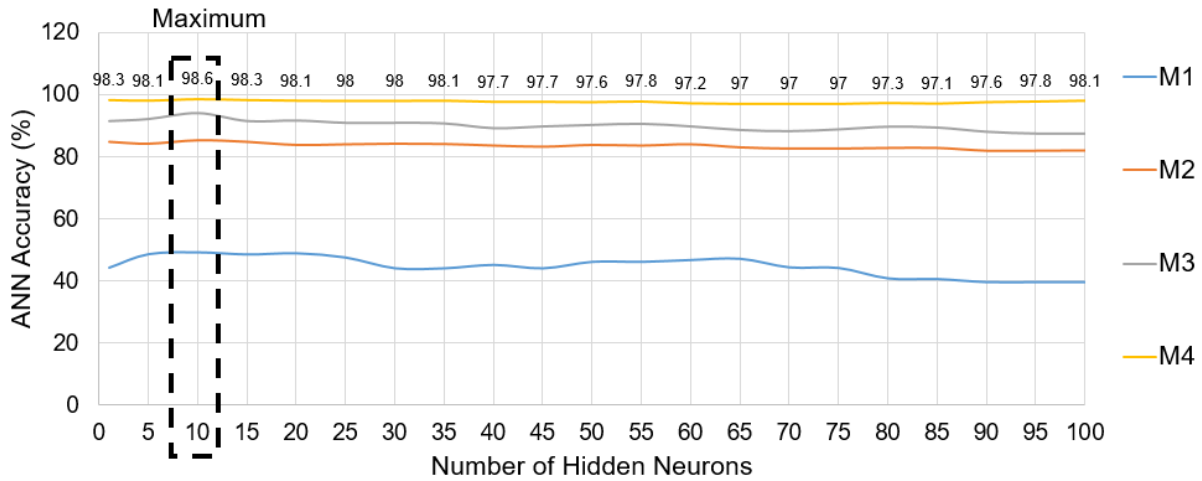
202 where  $\delta$  is the error function of the simulation process,  $w$  is the vector of the weights for the  
 203 developed ANN network shown in Figure 3, and  $s$  is the iteration number. The best layout of the  
 204 developed ANN network is also shown in Figure 4.

205 The developed structure of the ANN network is shown in Figure 4(a). The RBF network with two  
 206 inputs, one hidden layer and 10 hidden neurons is selected. In fact, the selection of the inputs was  
 207 obtained using the available parameters from dataset, including the solar irradiance ( $G$ ) and the  
 208 output power ( $P$ ). The selection of the hidden layers is obtained using an extensive simulation  
 209 from 1 to 100 hidden layers; as a result, ten hidden layers were selected due to its optimum  
 210 performance. The results of the ANN network accuracy vs the number of hidden neurons used for  
 211 the considered methodologies (M1, M2, M3, and M4) is shown in Figure 4(b). It is noticed that  
 212 the last adopted methodology achieved the highest ANN detection accuracy of 98.6% using 10  
 213 hidden neurons. The minimum ANN accuracy of 40.2% is observed for the first methodology  
 214 using 90-100 hidden neurons.





(a)



(b)

Figure 4. (a) Details of the proposed ANN network architecture, (b) ANN accuracy vs number of hidden neurons

216 **3.2 ANN Network Training and Validation**

217 Before the training and validation process began, the faulty conditions considered for the ANN to  
 218 detect had to be identified. In this article, 10 different scenarios have been taken into consideration,  
 219 presented as follows:

- 220 • Case 1: Normal operation mode, where no faults were applied to the PV string
- 221 • Case 2: 1 Fault applied to the system; 1 PV module disconnected from the PV string
- 222 • Case 3: 2 Faults applied to the system; 2 PV modules disconnected from the PV string
- 223 • Case 4: 3 Faults applied to the system; 3 PV modules disconnected from the PV string
- 224 • Case 5: 4 Faults applied to the system; 4 PV modules disconnected from the PV string
- 225 • Case 6: 5 Faults applied to the system; 5 PV modules disconnected from the PV string
- 226 • Case 7: 6 Faults applied to the system; 6 PV modules disconnected from the PV string
- 227 • Case 8: 7 Faults applied to the system; 7 PV modules disconnected from the PV string
- 228 • Case 9: 8 Faults applied to the system; 8 PV modules disconnected from the PV string
- 229 • Case 10: 9 Faults applied to the system; 9 PV modules disconnected from the PV string

230 It is worth noting that the partial shading considered in this research is when a PV module is  
 231 affected by either shading caused by moving clouds or when an overcasting weather condition is  
 232 arisen. Hence, no applied shading was practiced as we tried the best to comply with real shading  
 233 scenarios rather than using opaque objects like some research do. For that reason, we took long-  
 234 term data measurements of the PV installation over a period of 10 weeks, rather than simply reliant  
 235 on simulated or applied shading conditions which can be operated over couple hours.

236 Figure 5 shows a flowchart of the proposed fault detection architecture. Initially, the measured  
 237 output power of the PV string was attained using the MPPT unit. If the output power was greater  
 238 than zero, the measured power was passed into the developed ANN network. In case the output  
 239 was equal to zero, verification of the measured voltage had to be carried out to decide whether the  
 240 PV string was faulty (voltage > 0), or in sleep mode (V = 0).

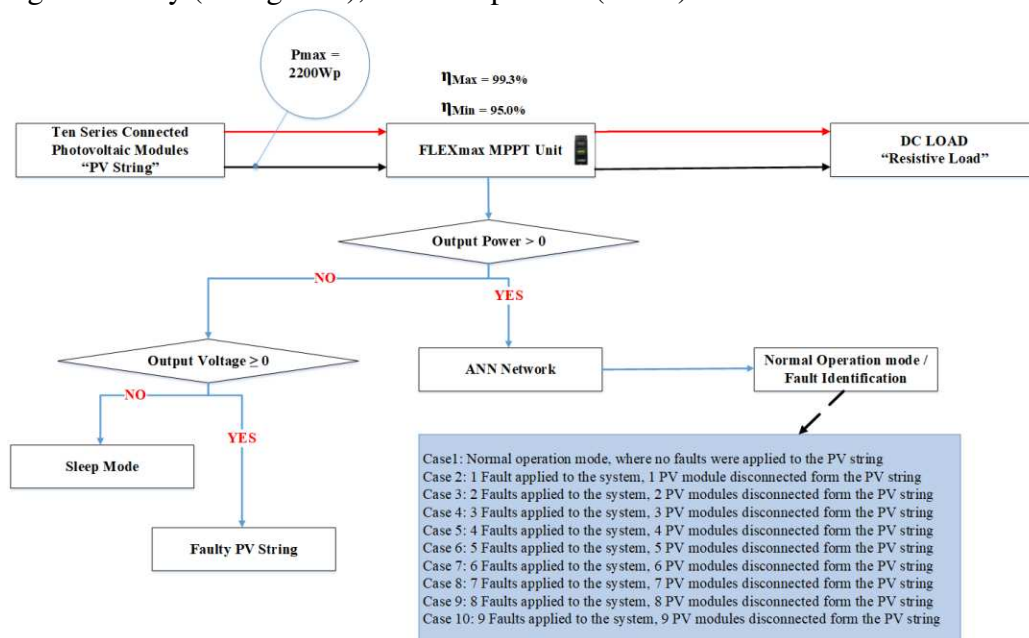
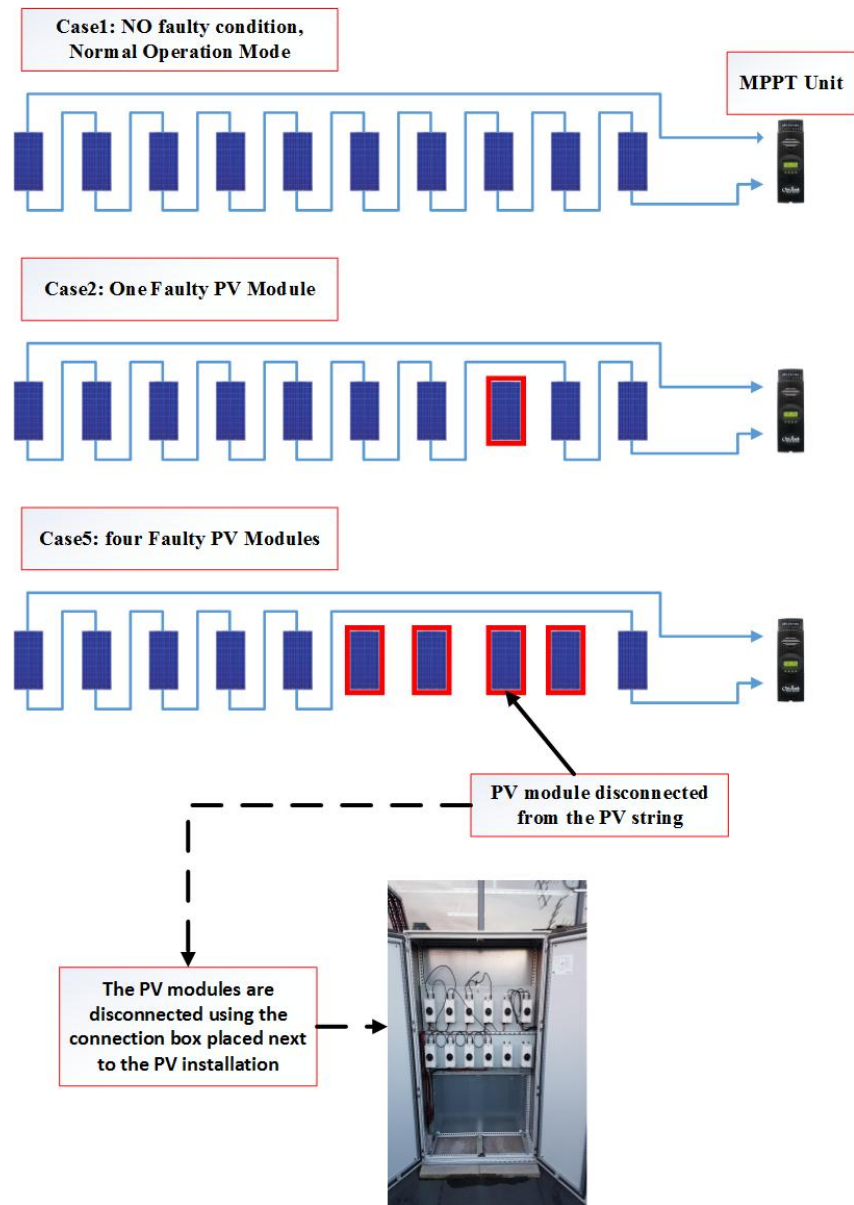


Figure 5. Flowchart of the proposed fault detection algorithm

241 In order to practically testify the examined faulty scenarios, we have used the junction-box placed  
242 next to the PV installation in which we can apply any faulty condition to the PV string, and this  
243 junction-box can be configured manually using a switch-connection where a PV module(s) can be  
244 connected or disconnected from the PV string.

245 For instance, Figure 6 shows three case scenarios applied to the PV installation including case 1  
246 “normal operational mode”, case 2 “one PV module is disconnected from the PV string”, and case  
247 5 “four PV modules are disconnected from the PV string”.



**Figure 6.** Schematic shows two applied cases on the examined PV installation

248 The data set used for training the ANN was recorded from the experimental PV setup shown  
 249 previously in Figure 2. During the experiments, the value of solar irradiance and total power were  
 250 logged, with the PV modules' temperature between 9.8 – 24.6 °C. As the proposed ANN model  
 251 does not require the temperature of the solar modules; hence, this value was not taken into  
 252 consideration. The data set shown in Figure 7 of the solar irradiance and the output power, consists  
 253 of 97200 measurements captured for 10 weeks. Each week corresponds to a different condition.

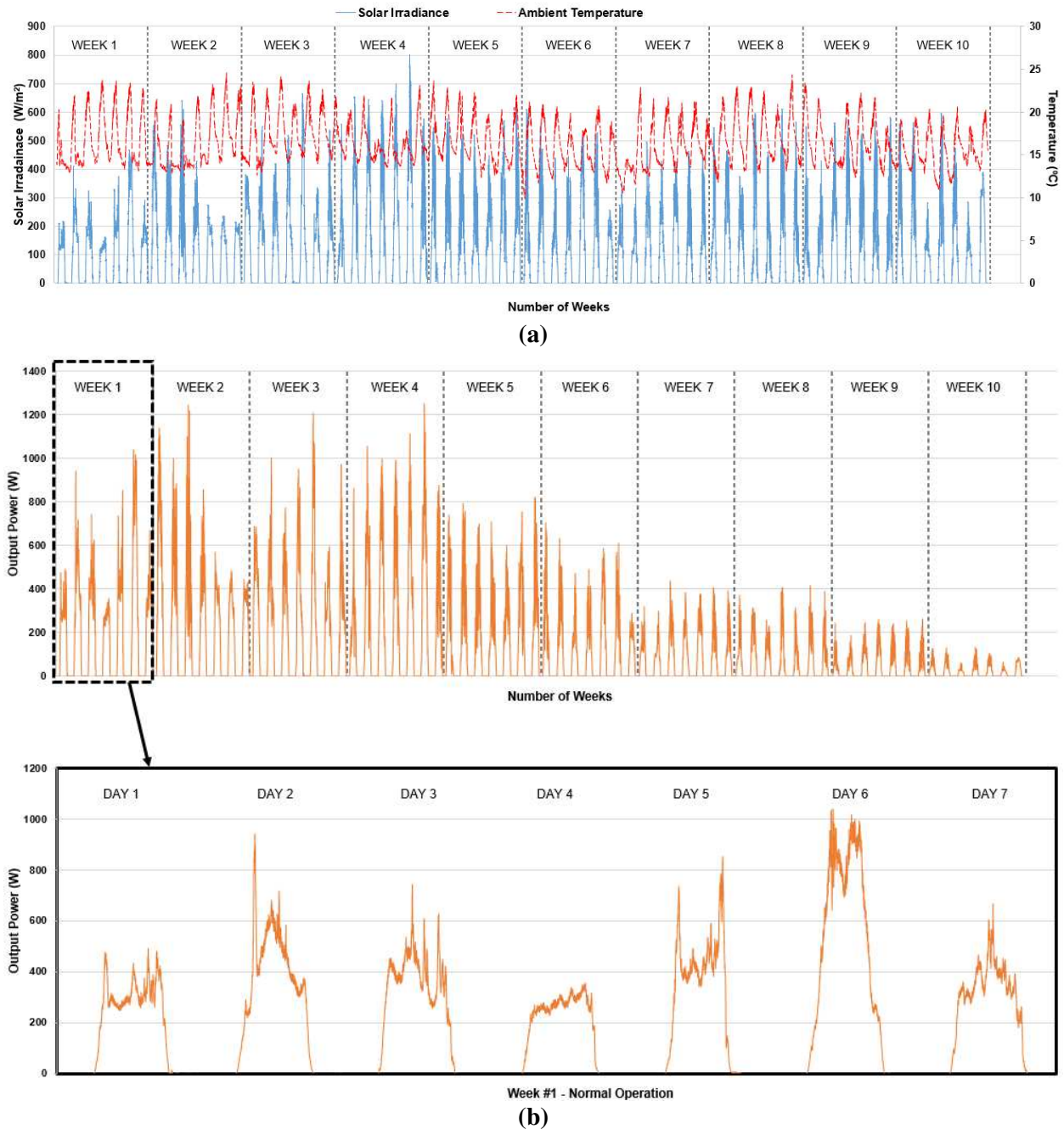


**Figure 7.** Data set used for training purposes; 97200 samples, each scenario has 9720 samples gathered over ten weeks. (a) Solar irradiance, (b) Output PV power

254 Various methodologies available in literature [5, 21, 24, and 26] used training samples for one to  
 255 three days for faulty conditions. While in our case, the data was recorded over a duration of one  
 256 week for every faulty condition. Another limitation of the recent work, 2019, conducted by [27  
 257 and 28] is that the ANN networks were trained using various inputs such as PV string voltage,  
 258 current, solar irradiance, power and ambient temperature. Whereas our proposed ANN network  
 259 only requires solar irradiance and output power as an input for the network. Note, a brief  
 260 comparison of the accuracy will be discussed later in section 5.

261 It is worth noting as the number of faults increases on a week-by-week basis, the total output power  
 262 measured for the PV system deteriorated, as shown in Figure 8.

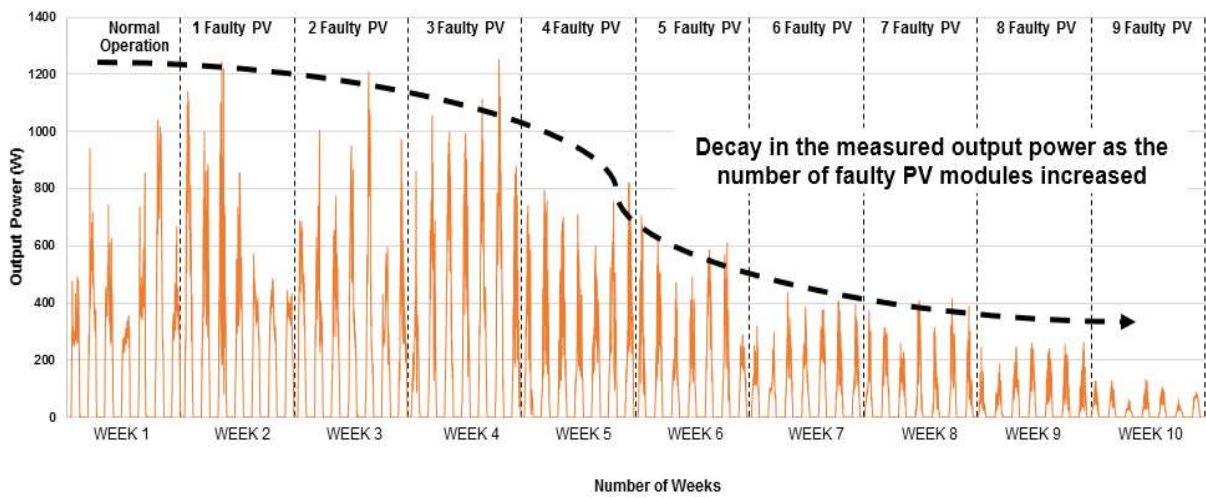


**Figure 8.** Flowchart of the proposed fault detection algorithm

263 As part of some methodologies (M3 and M4) which will be discussed in the following sub-  
 264 sections, the normalisation process of the input data for the solar irradiance and output power had  
 265 to be carried out.

266 The standard input parameters used to configure all tested ANN models are the solar irradiance  
 267 ( $G$ ) and total output power ( $P$ ). The Data set (input variables) are normalised using the max-min  
 268 normalisation technique, within the range of 0 and +1 using (5).

269 
$$y = \frac{(y_{\max} - y_{\min})(x - x_{\min})}{(x_{\max} - x_{\min})} + y_{\min} \quad (5)$$

270 where  $x \in \{x_{\min}, x_{\max}\}$  is the original data value, and  $y \in \{y_{\min}, y_{\max}\}$  is the corresponding  
 271 normalised value with  $y_{\min} = 0$  and  $y_{\max} = +1$ .

272

### 3.3 Implementation and Validation of the First Methodology (M1)

273

The ANN network was trained with randomly selected solar irradiance and output power, including non-representative data (represented by a zero for power), no normalisation of sample data was carried out in this approach. The ANN achieved an overall detection accuracy of 49.4%, refer to Figure 9(a). Many factors could have contributed to the low accuracy of the network. One possible factor was the inclusion of ‘non-representative’ data denoted by a zero, either for solar irradiance or PV output power.

279

### 3.4 Implementation and Validation of the Second Methodology (M2)

280

This methodology looks to improve the accuracy of the ANN by addressing the possible cause highlighted in M1. The input parameters (solar irradiance and output power) were randomly selected, but all ‘non-representative’ data was removed from the sample set which was to be used for training the network. The ANN network achieved an improved overall accuracy of 85.4%, refer to Figure 9(b). However, this is still considered as low accuracy for an ANN. This could have been due to no normalisation of data being carried out on the selected sample set.

286

For ANN networks training and validation, every dataset does not require normalisation. It is required only when features have different ranges. In our case, normalisation process would be expected to enhance the accuracy of the ANN as both ANN inputs, solar irradiance and output power, have a divergent range, i.e. the solar irradiance ranges from 0-1000 W/m<sup>2</sup>, while the output power ranges from 0 to 2200 W.

291

The green and red cells of the matrix represent the number of correct and incorrect classifications by the ANN, respectively. The grey cells represent the total detection accuracy with respect to each row and column. The number 1, represents 1- fault (F1) and so on, ending at 10- faults (F10).

292

293

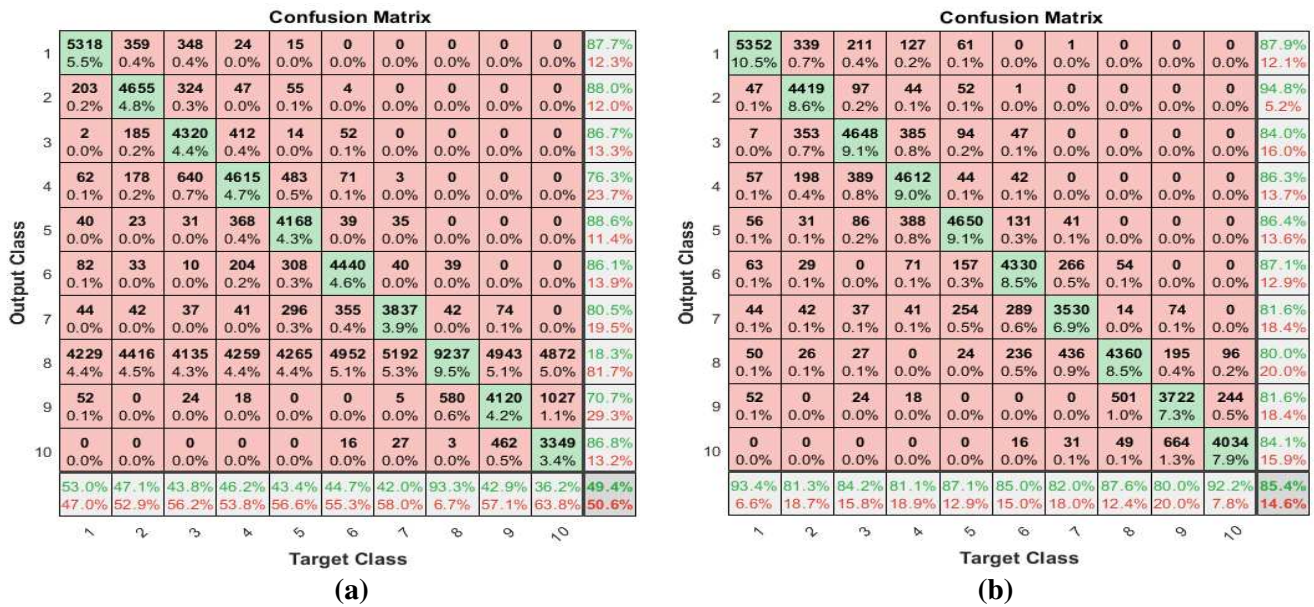


Figure 9. Output confusion matrix. (a) M1, (b) M2

294 **3.5 Implementation and Validation of the Third Methodology (M3)**

295 For the development of the third methodology, we have considered the previous methodologies  
 296 (M1 and M2), but also included the normalisation of the sample set data before training the ANN  
 297 network. The overall detection accuracy of the ANN using this approach was 94.2%, refer to  
 298 Figure 10. An improvement can be seen as compared to the above approaches due to the  
 299 normalisation of data before training the ANN. However, normalisation does not cater for missing  
 300 data samples between two data points. For example, the normalised data of the solar irradiance  
 301 may include values from 500 and 505 but not the values in between. This issue is further explored  
 302 in the implementation of the fourth ANN architecture.

**Confusion Matrix**

	1	2	3	4	5	6	7	8	9	10	
1	5292 10.4%	193 0.4%	129 0.3%	52 0.1%	4 0.0%	0 0.0%	0 0.0%	0 0.0%	0 0.0%	0 0.0%	93.3% 6.7%
2	100 0.2%	4937 9.7%	143 0.3%	22 0.0%	3 0.0%	0 0.0%	0 0.0%	0 0.0%	0 0.0%	0 0.0%	94.9% 5.1%
3	19 0.0%	44 0.1%	5108 10.0%	63 0.1%	17 0.0%	0 0.0%	0 0.0%	0 0.0%	0 0.0%	0 0.0%	97.3% 2.7%
4	8 0.0%	15 0.0%	43 0.1%	5160 10.1%	72 0.1%	13 0.0%	0 0.0%	0 0.0%	0 0.0%	0 0.0%	97.2% 2.8%
5	5 0.0%	19 0.0%	20 0.0%	66 0.1%	5250 10.3%	170 0.3%	20 0.0%	6 0.0%	9 0.0%	0 0.0%	94.3% 5.7%
6	0 0.0%	0 0.0%	0 0.0%	16 0.0%	71 0.1%	4584 9.0%	86 0.2%	35 0.1%	9 0.0%	0 0.0%	95.5% 4.5%
7	0 0.0%	0 0.0%	0 0.0%	0 0.0%	60 0.1%	55 0.1%	4485 8.8%	60 0.1%	18 0.0%	0 0.0%	95.9% 4.1%
8	0 0.0%	0 0.0%	0 0.0%	10 0.0%	15 0.0%	8 0.0%	236 0.5%	4699 9.2%	80 0.2%	18 0.0%	92.8% 7.2%
9	0 0.0%	0 0.0%	0 0.0%	0 0.0%	10 0.0%	11 0.0%	31 0.1%	79 0.2%	4142 8.1%	312 0.6%	90.3% 9.7%
10	0 0.0%	0 0.0%	0 0.0%	0 0.0%	4 0.0%	39 0.1%	22 0.0%	55 0.1%	347 0.7%	4511 8.8%	90.6% 9.4%
	97.6% 2.4%	94.8% 5.2%	93.8% 6.2%	95.8% 4.2%	95.4% 4.6%	93.9% 6.1%	91.9% 8.1%	95.2% 4.8%	89.9% 10.1%	93.2% 6.8%	94.2% 5.8%
	1	2	3	4	5	6	7	8	9	10	
	<b>Target Class</b>										

Figure 10. Output confusion matrix obtained using M3

303 **3.6 Implementation and Validation of the Fourth Methodology (M4)**

304 The normalised data of the solar irradiance or output power may include value, for example, 500  
 305 and 505 but not the values in between. This method implemented the concept of ‘mapping’ sample  
 306 data set, before feeding it into the ANN for training, validating and testing purposes. Through the  
 307 implementation of mapping input parameters, all values within the defined data points are taken  
 308 into account. The ANN was trained using randomly selected data set, no “off-state” data was  
 309 involved, normalisation process had been implemented, and finally the novel part of this approach,  
 310 the mapping feature of the solar irradiance against the PV system output power was implemented.

311 The solar irradiance 0 - 1000 W/m<sup>2</sup> was mapped along with the corresponding output power as  
 312 shown in Figure 11(a), with a step size of 1 W/m<sup>2</sup>. The accuracy of the ANN improved  
 313 significantly (98.6%) compared to the prior methods, as presented in Figure 11(b).

314 As suggested, the rationale behind the mapping of the inputs was to try and obtain a complete  
 315 dataset before training the network. This was made possible due to only having two inputs.  
 316 However, datasets containing multiple variables such as temperature, wind speed, voltage along  
 317 with irradiance and power would make the task more difficult.

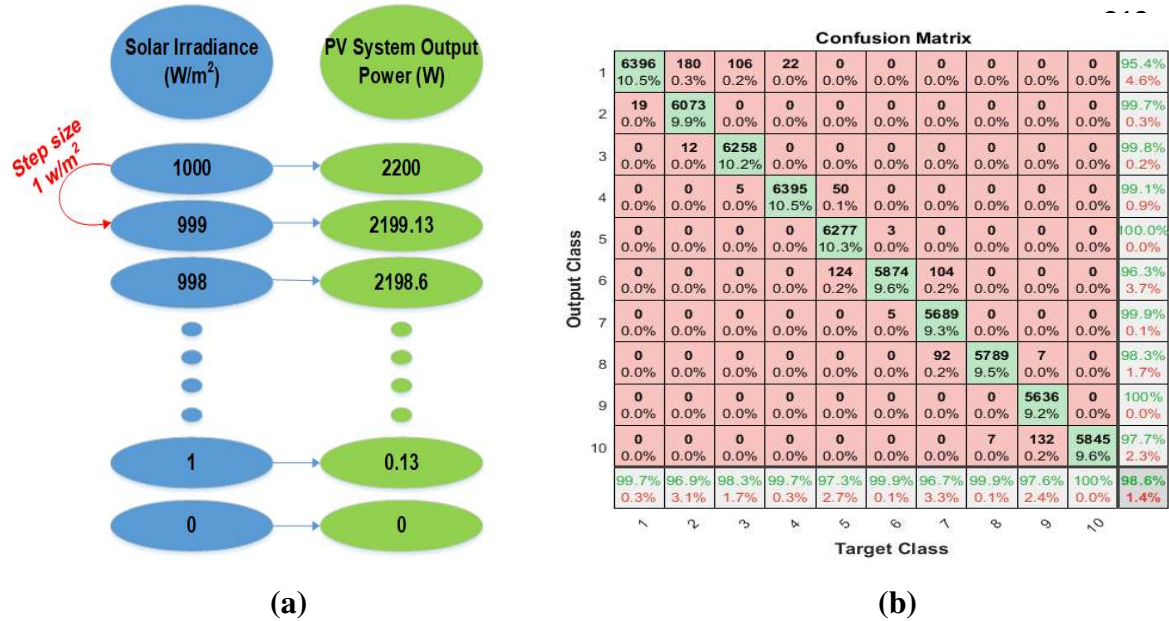


Figure 11. (a) Mapping solar irradiance and PV system output power, (b) Confusion Matrix for M4

### 329 3.7 Evaluation of the Four Developed Methodologies

330 The overall detection accuracy of the ANN based on the four methodologies is presented in Table  
 331 2. A key observation to take away from Table 2, is the importance of data normalisation before  
 332 proceeding with the training of the ANN. M1, had the least detection accuracy (49.4%). This was  
 333 primarily because the raw data extracted from the PV setup shown in Figure 2, was directly used  
 334 to train the ANN without filtering noisy data. The dismissal of ‘off-state’ data (M2), significantly  
 335 improved the accuracy of the network (85.4%). Normalisation (M3), further improved the  
 336 detection accuracy (92.2%) thanks to the sync of the input range, with (M4) achieving the highest  
 337 detection accuracy due to the mapping of inputs to cater for missing data points.

Table 2. Evaluating all developed methodologies

Methodology No.	Training data set including solar irradiance and output power	Training Data does not include “off-state” samples	Normalisation Process of the training data set	Mapping 0-1000 W/m <sup>2</sup> into the actual output power	ANN network detection accuracy (%)
M1	✓	✗	✗	✗	49.4
M2	✓	✓	✗	✗	85.4
M3	✓	✓	✓	✗	92.2
M4	✓	✓	✓	✓	98.6



338 The critical element in increasing the ANN-network detection accuracy is principally due to the  
 339 increase of the ANN receiver operating characteristics (ROC) during the training, validation and  
 340 testing stages. The ROC is a graph showing the performance of a classification model at all  
 341 classification scenarios (i.e. class 1 corresponds to case1 “normal operation mode”, while class 10  
 342 corresponds to case 10 “9 faulty PV modules”).

343 As can be noticed in Figure 12(a), during the training and validation of methodology 1, the ROC  
 344 tends to have a high false-positive rate which at the end reduces the overall detection accuracy of  
 345 the ANN network. Comparatively, Figure 12(d) shows the ROC for the last methodology, while it  
 346 is evident that the true-false rate has significantly decreased, there is an increase in the true-positive  
 347 rate due to the impact of the normalisation and the mapping procedure implemented during the  
 348 data handling processing stage, resulting in the highest rate of detection accuracy of 98.6%.

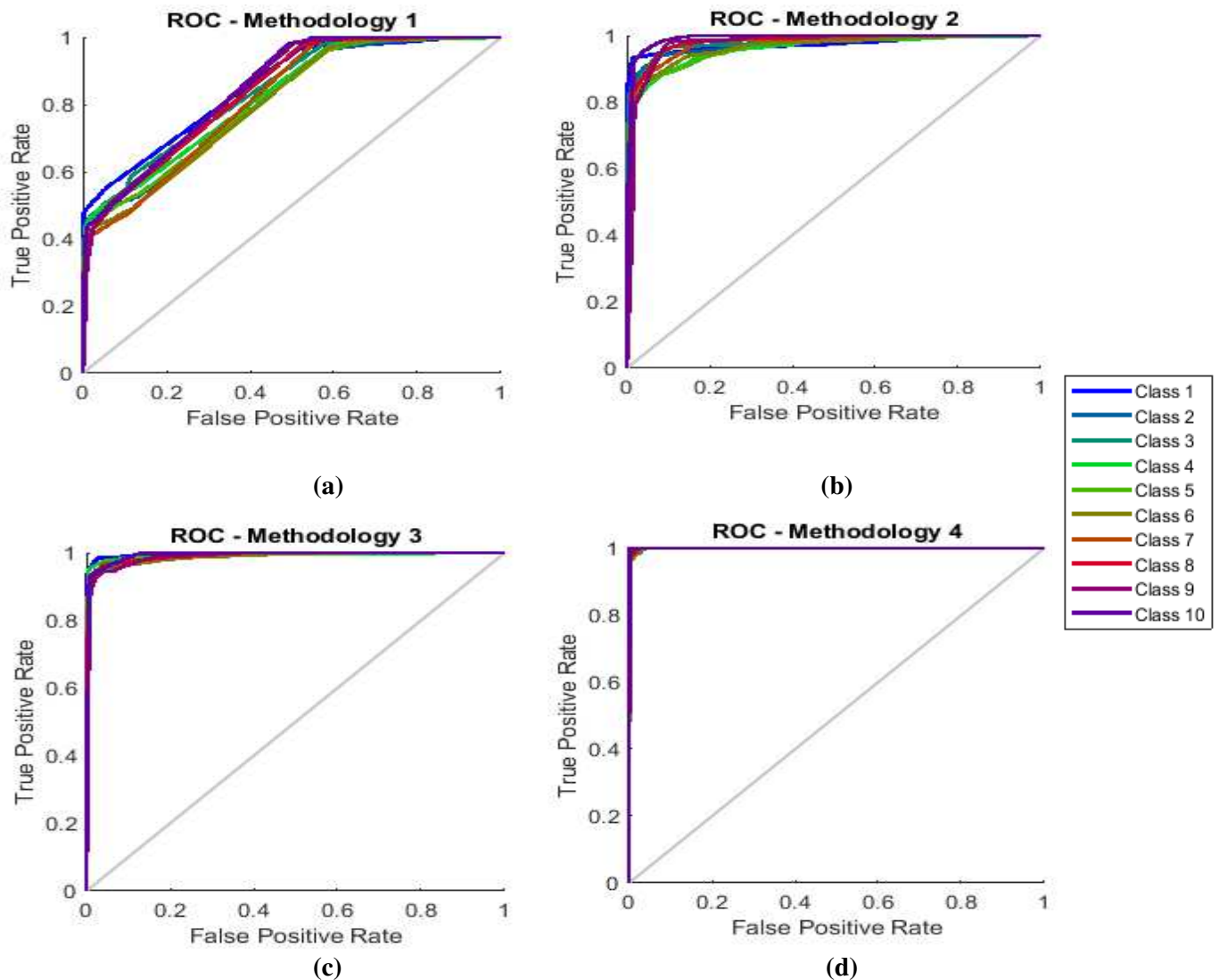


**Figure 12.** ROC performance of each ANN methodology. (a) M1, (b) M2, (c) M3, (d) M4

349 According to what has been discussed so far, it is worth noting that the rationale for the selection  
350 of RBF over Multilayer perceptron networks (MLP) was due to the network only requiring a single  
351 hidden layer but more importantly due to RBF's robustness to adversarial samples in the data set.  
352 As proven in this section, the ANN architecture accuracy was compared with a varying number of  
353 hidden layers. The results showed that a single hidden layer was the most optimal solution  
354 providing an accuracy of almost 99%. As a result of this an RBF network was selected rather than  
355 an MLP. Although MLP can also be used in a single hidden layer configuration, it demands more  
356 computational power.

357 The first novelty this research brings to the field of PV fault detection through ANN, is the use of  
358 only two inputs for training the network, i.e. solar irradiance and output power. While the authors  
359 acknowledge that the introduction of smart meters provide an effective platform for obtaining  
360 various inputs used for training ANN, without having major implications in terms of more  
361 hardware, there are other issues which are introduced as a result. The use of, for example, a five  
362 inputs ANN-based fault detection system rather than two means more time must be spent on data  
363 processing. It is, in fact, this stage of the process in the development of an ANN which directly  
364 impacts the overall accuracy of the network. If the network requires five inputs, the smart meter  
365 will be able to provide this data, but the problem occurs when the data must be processed for  
366 training the network as additional inputs result in more time required for data censoring and higher  
367 chances of non-representative data making its way into the network due to human error. Whereas,  
368 by limiting the inputs to only two, as proposed in this article, less time and effort is required for  
369 data processing, less chances of noisy data leaking into the training stage and ultimately a higher  
370 performing network, as evident from section 4.

371 In addition, as we have used solar irradiance data, academics, industry and national interest alike  
372 are demanding this data for various reasons such as predicting the ambient temperature, techno-  
373 economic analysis of the heating systems, transportation sector, etc. Therefore, we do not consider  
374 acquiring solar irradiance is a major drawback of this research, since, as an example, the UK Met-  
375 office<sup>1</sup> have a live grid climate variable system to download live solar irradiance as well as  
376 forecasted data; this approach of making live data for public use is now widely held in various  
377 counties such as Spain, Italy, and Singapore.

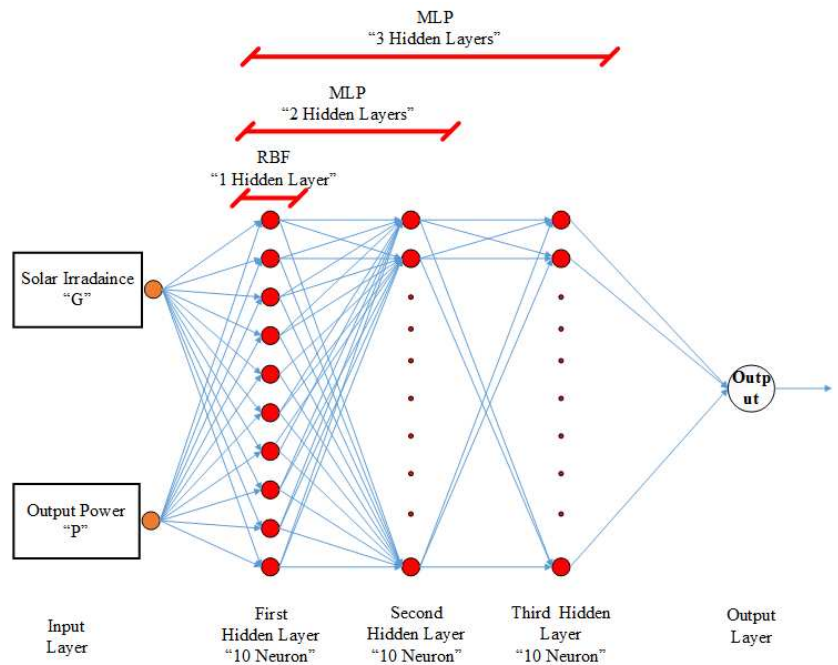
378 Another novel part of this research (principally using the fourth methodology) is the mapping of  
379 the inputs after removing non-representative data and carrying out data normalisation. A  
380 fundamental component within this methodology which plays a vital role in achieving high  
381 accuracy is the selection of the 'step size' for the mapping. A step size of 'one' was selected as  
382 shown in Figure 11. The rationale for not selecting a step size of '10' was due to under-fitting. As  
383 the gap between the data points would make it difficult for the network to be able to generalize.  
384 Conversely, a step size of less than one, for example '0.5', would force the network to accurately  
385 map the data points without generalizing, resulting in a network that is unable to accurately classify  
386 new input data, rendering it as an 'over-fit' network.

<sup>1</sup><https://www.metoffice.gov.uk/research/climate/maps-and-data/data/haduk-grid/haduk-grid>

387 **3.8 RBF vs. MLP**

388 RBF and Multi-Layer Perceptron (MLP) are both neural networks as shown in Figure 13. Both  
389 networks have some common features but also significant differences in the way they operate,  
390 which makes one network more suited for certain applications as compared to the other. The well-  
391 known difference between the two networks is that RBF only uses a single hidden layer, whilst  
392 MLP can accommodate multiple hidden layers.

393 Both RBF and MLP networks can be used for regression and classification problems. Also, both  
394 networks have the capability to approximate complicated functions. However, RBF's have explicit  
395 local representations as each neuron represents a specific region of the input space. Conversely, in  
396 an MLP network, each neuron tries to  
397 capture a specific feature from the  
398 training set. Early neuron layers  
399 capture low-level features and as the  
400 information propagates through the  
401 hidden layers the feature extraction  
402 matures. This can optimize the  
403 overall accuracy of the network but at  
404 the expense of increased  
405 computational power, a trade-off  
406 which comes down to the objectives  
407 of the project. As there is only one  
408 hidden layer in an RBF network, each  
409 neuron captures the similarity  
410 between the whole training set and  
411 the center of the Euclidian.



412 **Figure 13. RBF vs. MLP**

413 Moreover, the RBF is more adequate compared with the MLP is due to the digital nature of the  
414 failure associated with the PV system; the individual PV modules are completely "ok" or  
415 completely "off", where no "intermediate" failure occurs.

416 The selection of the ANN network was based on the results obtained from testing and comparison  
417 of the two networks in terms of the overall detection accuracy and required computational time.  
418 Figures 14 (a) and (b), show the overall detection accuracy of two MLP networks with 2 and 3  
419 hidden layers, respectively. There is only a small difference in the accuracy (+0.2%) whereas the  
420 computational time increased by 155ms, refer to Figure 14 (c).

421 When comparing an RBF with an MLP network consisting of 3 hidden layers the detection  
422 accuracy increased by a small margin (+0.5%) whilst the corresponding computational time

423 increased considerably from 45ms to 290ms. Consequently, increasing the time of which a PV  
 424 fault can be detected as well as the overall energy consumption of the microcontroller power unit.

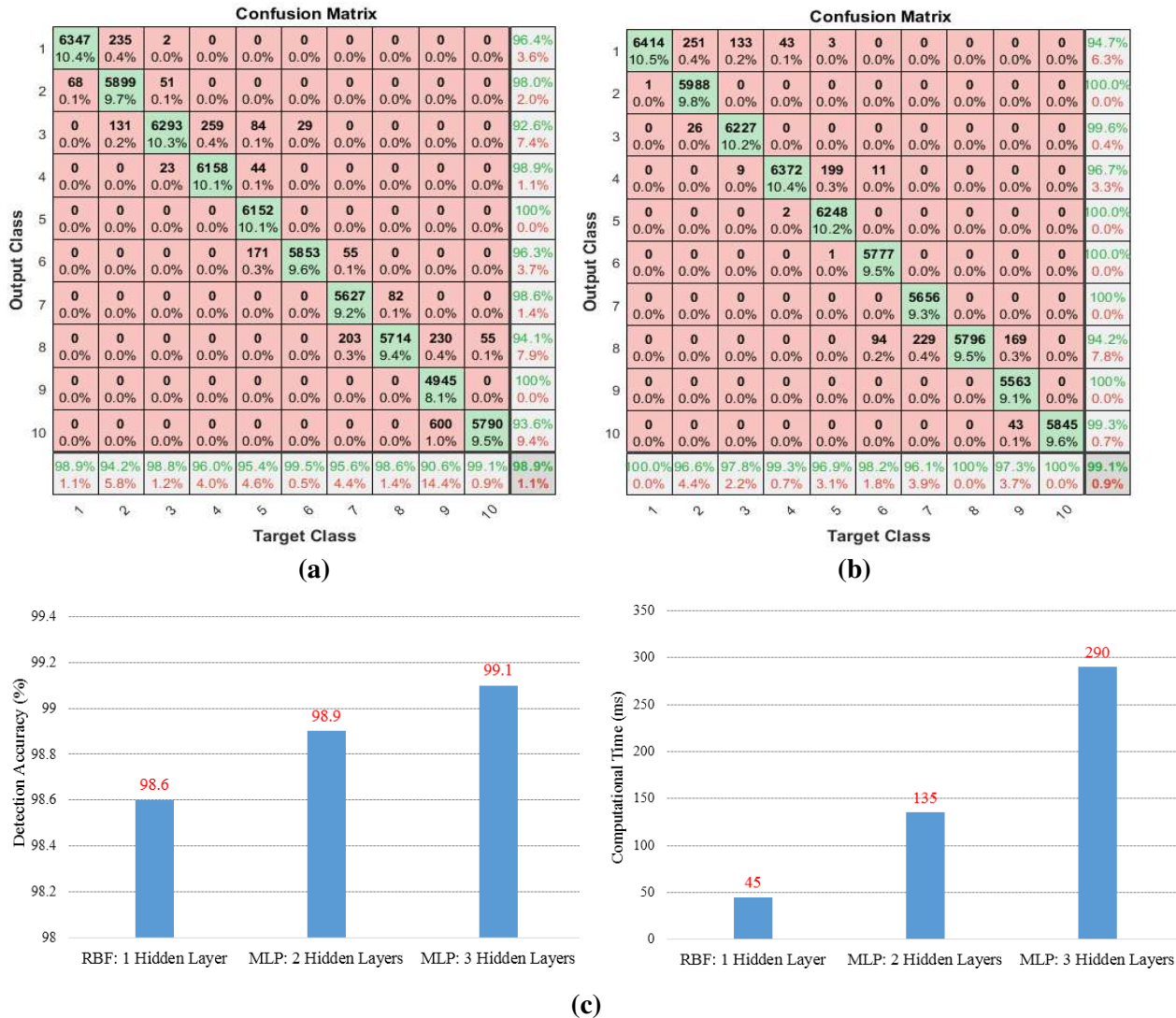


**Figure 14.** Output detecting accuracy of the MLP networks vs. RBF network. (a) 2 hidden layers, (b) 3 hidden layers, (c) Detection accuracy and the minimum computational time difference

425 **3.9 t-test statistical analysis**

426 In practice, comparing the competence of ANN models with conventional statistical techniques is  
 427 critical, as uncomplicated statistical models could result the same detection accuracy compared  
 428 with complicated ANN models. Therefore, we have used the well-established t-test technique that  
 429 uses the mean value of two tests (in our case normal operation vs number of faulty PV module)  
 430 and resulting a t-test value, this test has been verified using Minitab software.

431 With a confidence of 99%, in theory, if the t-test value is greater than 2.58, therefore, there is a  
 432 significant difference in the two tested value, therefore a fault is ascertained in the PV system.

433 During no shading conditions, two tests were performed, including one faulty and nine faulty PV  
 434 modules in the PV string, results are shown in Figures 15(a) and (b). It is clearly notable that the  
 435 t-test is beyond the limit of 2.58, therefore a fault is detected in the PV string.

436 Whistle testing the same faulty conditions under partial shading condition, the result of the t-test  
 437 does not show a significant difference, as the t-test value is still within the theoretical threshold of  
 438 2.58 as can ben seen in Figures 15(c) and (d). This result confirms that even sophisticated statistical  
 439 technique such as t-test can only be used in some cases to detect the faults in the PV string, while,  
 440 for example, under shading conditions, it fails to determine the difference between the normal  
 441 operation and one faulty or nine faulty PV modules.

442 In conclusion, ANN model is therefore having a benefit over statistical-based techniques, as ANN  
 443 models can determine the difference of the power and irradiance levels and has the possibility to  
 444 distinguish the variations of these parameters including shading and non-shading conditions.

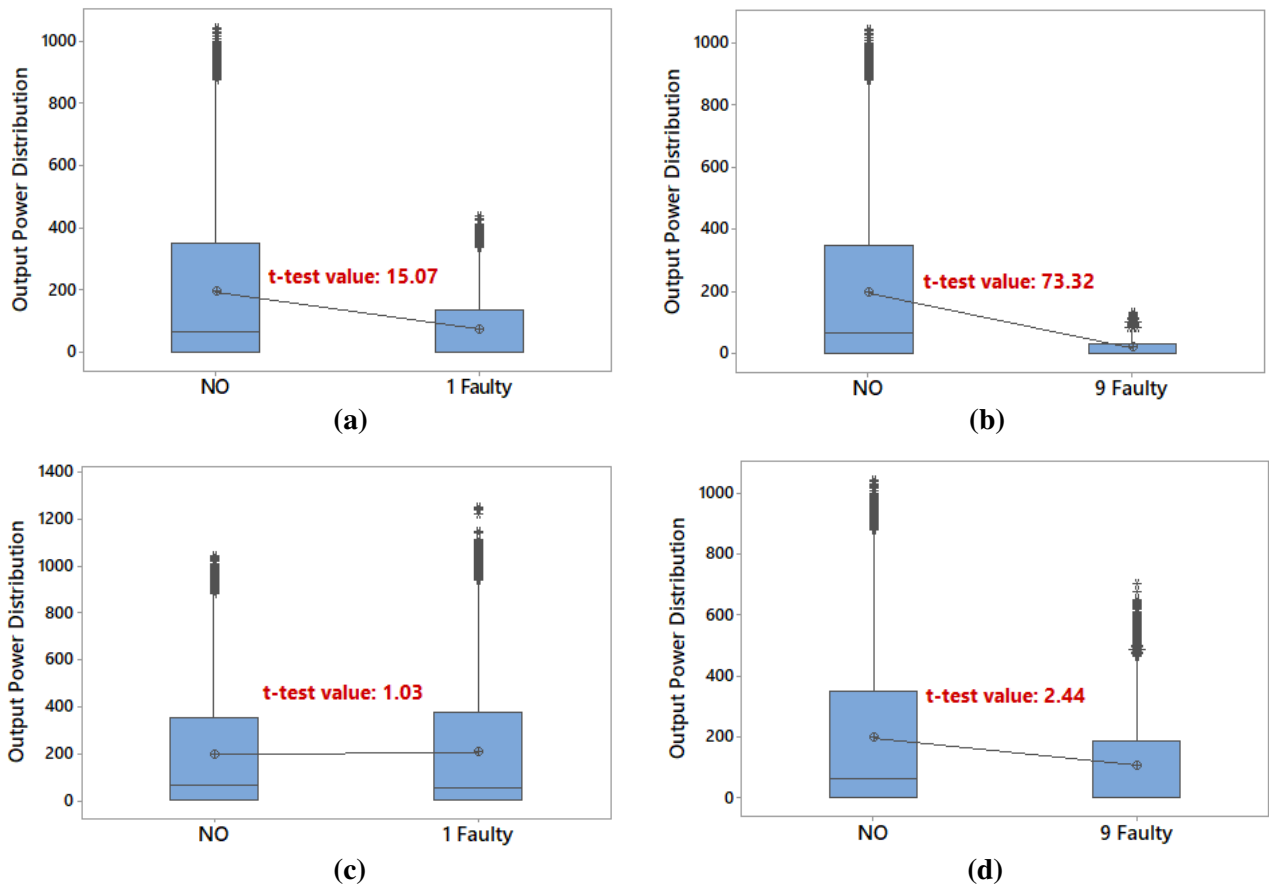


**Figure 15.** Output t-test value. (a) Normal operation vs one faulty PV module, without partial shading “sunny day”, (b) Normal operation vs nine faulty PV modules in the PV string, without partial shading, (c) Normal operation vs one faulty PV module, data captured under partial shading scenario, (d) Normal operation vs nine faulty PV modules in the PV string, without partial shading

445 **4. Results**

446 This section reports on the accuracy of the ANN through the implementation of the selected  
447 methodology (M4) from section 3.6, as this methodology had achieved the highest fault detection  
448 accuracy. Furthermore, the developed ANN using M4 is trained with a ‘scaled-up’ PV system and  
449 reduced data set, refer to section 4.3. Note that the data presented in this section for testing the  
450 actual accuracy of the ANN has not been previously used for training the ANN network, previously  
451 discussed in section 3, reiterating the authenticity and integrity of our ANN.

452 **4.1. Partial shading results**

453 The developed fault detection algorithm was subject to various experiments, in order to validate  
454 its resilience, robustness and accuracy. The sample-set was collected over two weeks with the first  
455 week testing under partial shading conditions and the latter under overcast conditions. Each  
456 scenario persists for an entire day with a different fault applied to the examined PV system  
457 illustrated previously in Figure 2.

458 The first week was based on validating the accuracy of the network based on the data collected on  
459 partial shading. The solar irradiance for week-one is represented in Figure 16.

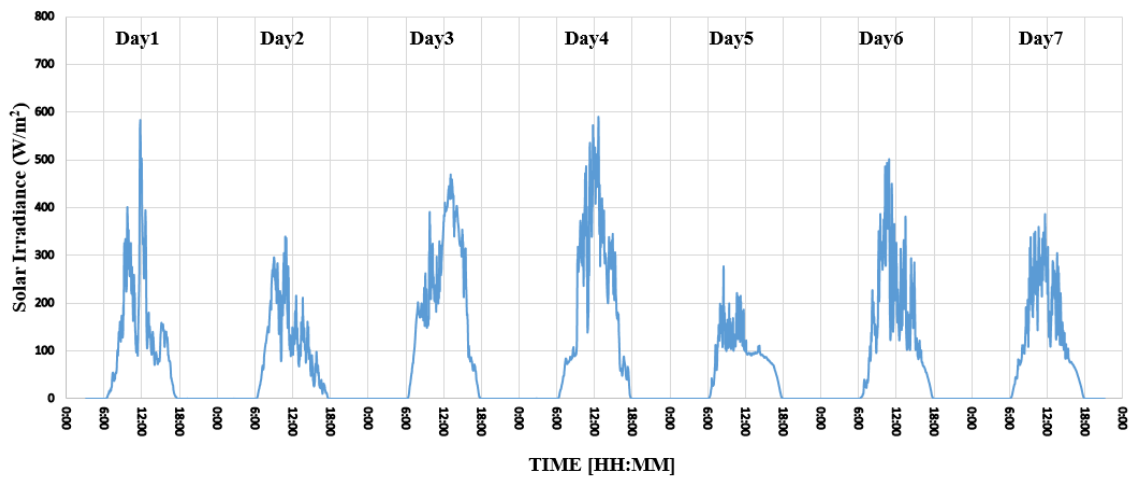


**Figure 16.** Solar irradiance of PV system for week one under partial shading conditions

460 The total output power of the system in question under different test conditions is represented in  
461 Figure 17. The system is operating without any applied faults on the first day; hence, the total  
462 output power is at its peak. During the duration of the week, as various faults are applied on a day  
463 to day basis, the total output power decays. With the system generating its lowest output power on  
464 day 6 with 7 faults applied. Note day-five has a low output power even though the system is  
465 running without any applied faults, and this is due to the corresponding solar irradiance being at  
466 its lowest for that day, represented in Figure 16.

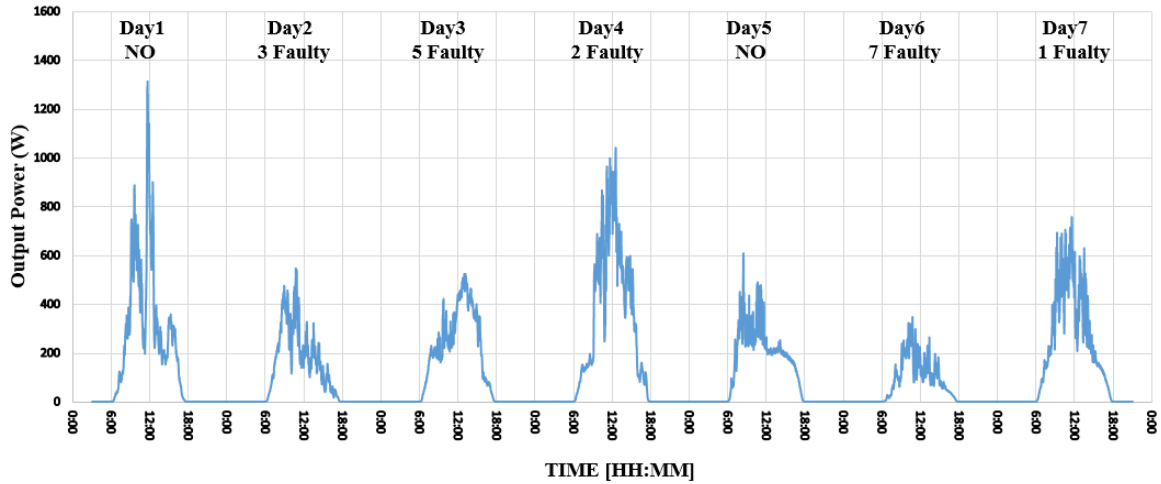


**Figure 17.** Total output power of PV system for week one under partial shading conditions

467 The authentication of the accuracy of the developed ANN under partial shading conditions over  
 468 the week is represented by the output classification matrices, shown in Figure 18. The green and  
 469 red cells of the matrix represent the number of correct and incorrect classifications by the ANN,  
 470 respectively. The grey cells represent the total detection accuracy with respect to each row and  
 471 column.

472 The overall accuracy of the system under partial shading conditions was 97.9%, as shown in Figure  
 473 18. Out of 1413 samples, there are 1373 samples for NO (normal operation) correctly classified,  
 474 whereas 40 samples are misclassified as F2, F3 or F4, this corresponds to 2.8% faulty  
 475 classifications during NO and shading conditions. On the other hand, 666 samples are correctly  
 476 classified as F2, while some samples are misclassified as either F1 or F3, this is due to the change  
 477 of the solar irradiance affecting the PV system during the fourth examined day.

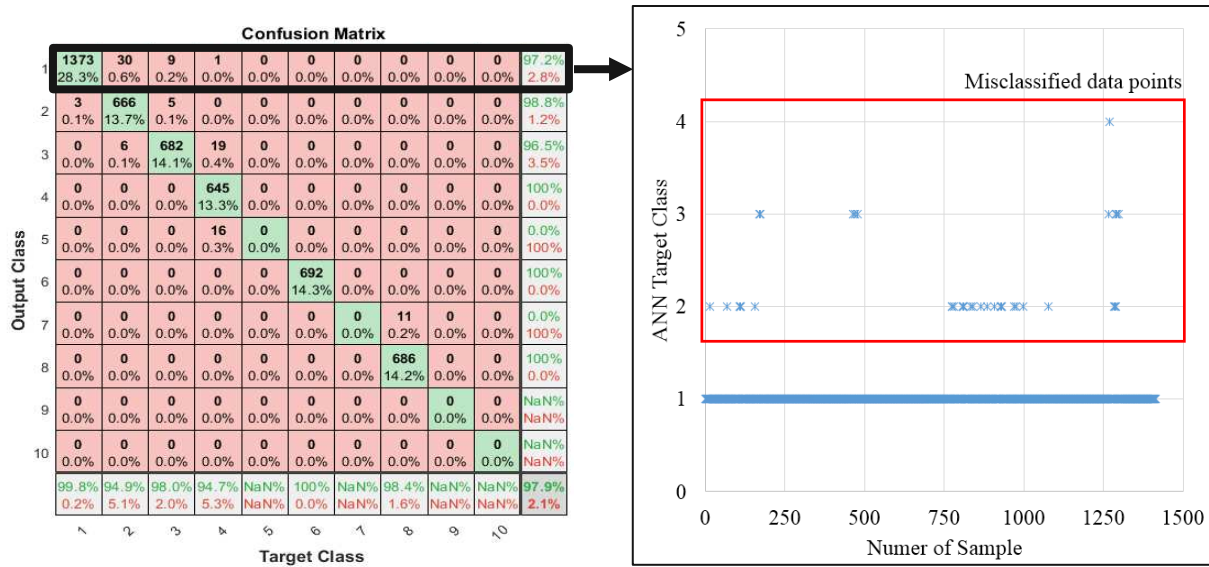


**Figure 18.** Confusion Matrix for ANN under partial shading conditions

478 **4.2. Overcast Results**

479 The second week was based on validating the accuracy of the network with regards to the data  
480 collected for overcast conditions (partially cloudy and overcast). The solar irradiance for week one  
481 is shown in Figure 19.

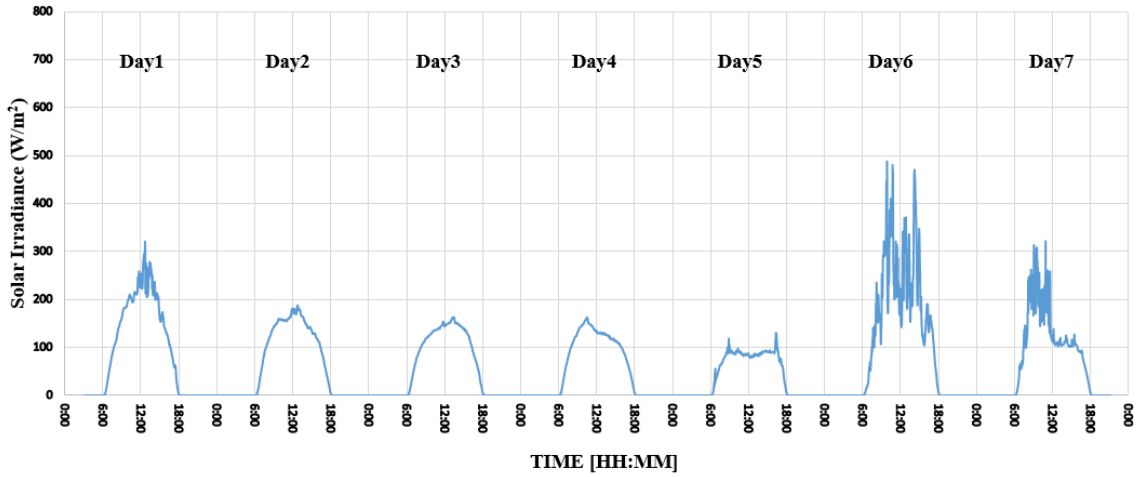


**Figure 19.** Solar irradiance of PV system for week two under overcast conditions

482 The total output power of the system in question under different test conditions is represented in  
483 Figure 20. The system is operating without any applied faults (normal operation) on the first day,  
484 but the total output power is not at its peak, whereas for the sixth day 1-fault is applied but it has  
485 the highest total output power for the week, this is due to the solar irradiance being significantly  
486 higher on day-six as compared to any other day of the week, including day-one.

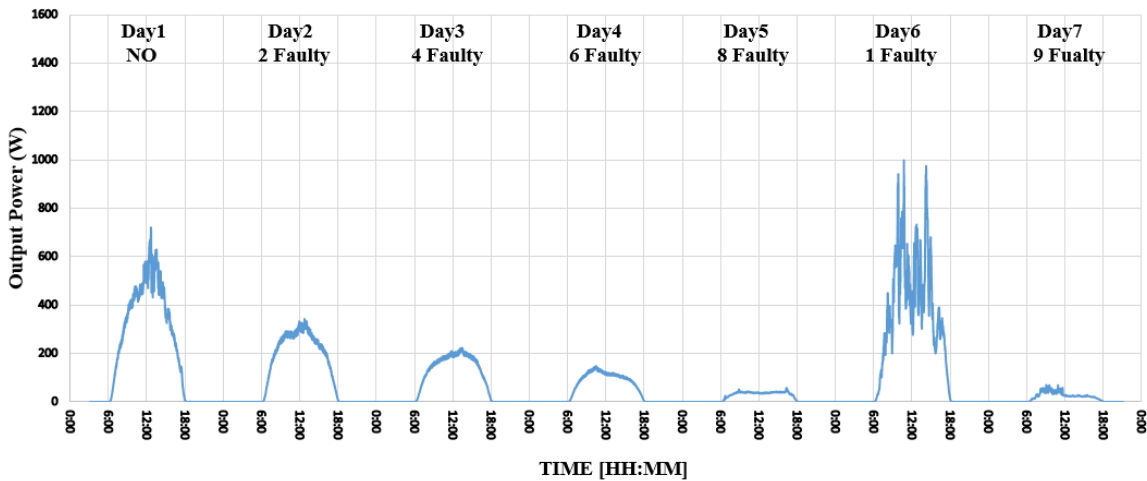


**Figure 20.** Total output power of PV system for week two under overcast conditions



487 As shown in Figure 21, the overall accuracy of the system for overcast conditions was 96.5%.  
 488 Total of 710 samples for normal operation “NO” are correctly classified. This corresponds to  
 489 14.2% of all tested samples. Similarly, 661 samples are correctly classified as F2, corresponding  
 490 to 13.2% of all samples. In row 1, 34 samples of NO are incorrectly classified as F1 corresponding  
 491 to 0.7%. This was because the output power during normal operation mode and 1-faulty PV  
 492 module are similar, particularly during partial shading conditions.

**Confusion Matrix**

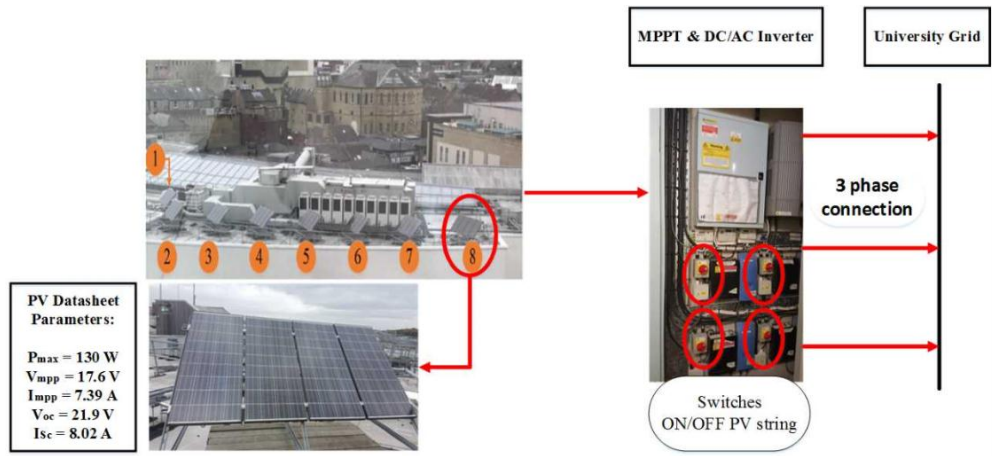
Output Class	1	710 14.2%	34 0.7%	0 0.0%	0 0.0%	0 0.0%	0 0.0%	0 0.0%	0 0.0%	0 0.0%	0 0.0%	0 0.0%	0 0.0%	0 0.0%	0 0.0%	0 0.0%	0 0.0%	0 0.0%	0 0.0%	710 95.4%	34 4.6%			
	2	5 0.1%	661 13.2%	0 0.0%	0 0.0%	0 0.0%	0 0.0%	0 0.0%	0 0.0%	0 0.0%	0 0.0%	0 0.0%	0 0.0%	0 0.0%	0 0.0%	0 0.0%	0 0.0%	0 0.0%	0 0.0%	0 0.0%	0 0.0%	661 99.2%	5 0.8%	
	3	0 0.0%	20 0.4%	711 14.2%	0 0.0%	12 0.2%	0 0.0%	0 0.0%	0 0.0%	0 0.0%	0 0.0%	0 0.0%	0 0.0%	0 0.0%	0 0.0%	0 0.0%	0 0.0%	0 0.0%	0 0.0%	0 0.0%	0 0.0%	0 0.0%	711 95.7%	20 4.3%
	4	0 0.0%	0 0.0%	2 0.0%	0 0.0%	3 0.1%	0 0.0%	0 0.0%	0 0.0%	0 0.0%	0 0.0%	0 0.0%	0 0.0%	0 0.0%	0 0.0%	0 0.0%	0 0.0%	0 0.0%	0 0.0%	0 0.0%	0 0.0%	0 0.0%	0 0.0%	2 0.0%
	5	0 0.0%	0 0.0%	0 0.0%	0 0.0%	678 13.5%	0 0.0%	0 0.0%	0 0.0%	0 0.0%	0 0.0%	0 0.0%	0 0.0%	0 0.0%	0 0.0%	0 0.0%	0 0.0%	0 0.0%	0 0.0%	0 0.0%	0 0.0%	0 0.0%	0 0.0%	678 100%
	6	0 0.0%	0 0.0%	0 0.0%	0 0.0%	27 0.5%	0 0.0%	7 0.1%	0 0.0%	0 0.0%	0 0.0%	0 0.0%	0 0.0%	0 0.0%	0 0.0%	0 0.0%	0 0.0%	0 0.0%	0 0.0%	0 0.0%	0 0.0%	0 0.0%	0 0.0%	27 100%
	7	0 0.0%	0 0.0%	0 0.0%	0 0.0%	0 0.0%	0 0.0%	683 13.6%	0 0.0%	0 0.0%	0 0.0%	0 0.0%	0 0.0%	0 0.0%	0 0.0%	0 0.0%	0 0.0%	0 0.0%	0 0.0%	0 0.0%	0 0.0%	0 0.0%	0 0.0%	683 100%
	8	0 0.0%	0 0.0%	0 0.0%	0 0.0%	0 0.0%	0 0.0%	27 0.5%	0 0.0%	33 0.7%	7 0.1%	0 0.0%	0 0.0%	0 0.0%	0 0.0%	0 0.0%	0 0.0%	0 0.0%	0 0.0%	0 0.0%	0 0.0%	0 0.0%	0 0.0%	27 100%
	9	0 0.0%	0 0.0%	0 0.0%	0 0.0%	0 0.0%	0 0.0%	0 0.0%	0 0.0%	0 0.0%	686 13.7%	0 0.0%	0 0.0%	0 0.0%	0 0.0%	0 0.0%	0 0.0%	0 0.0%	0 0.0%	0 0.0%	0 0.0%	0 0.0%	0 0.0%	686 100%
	10	0 0.0%	0 0.0%	0 0.0%	0 0.0%	0 0.0%	0 0.0%	0 0.0%	0 0.0%	0 0.0%	0 0.0%	0 0.0%	0 0.0%	0 0.0%	0 0.0%	0 0.0%	0 0.0%	0 0.0%	0 0.0%	0 0.0%	0 0.0%	711 14.2%	0 0.0%	
			99.3% 0.7%	92.4% 7.6%	99.7% 0.3%	NaN% NaN%	94.2% 5.8%	NaN% NaN%	95.3% 4.7%	NaN% NaN%	95.4% 4.6%	99.0% 1.0%	96.5% 3.5%											
		1	2	3	4	5	6	7	8	9	10													
		Target Class																						

**Figure 21.** Confusion Matrix for ANN under overcast conditions

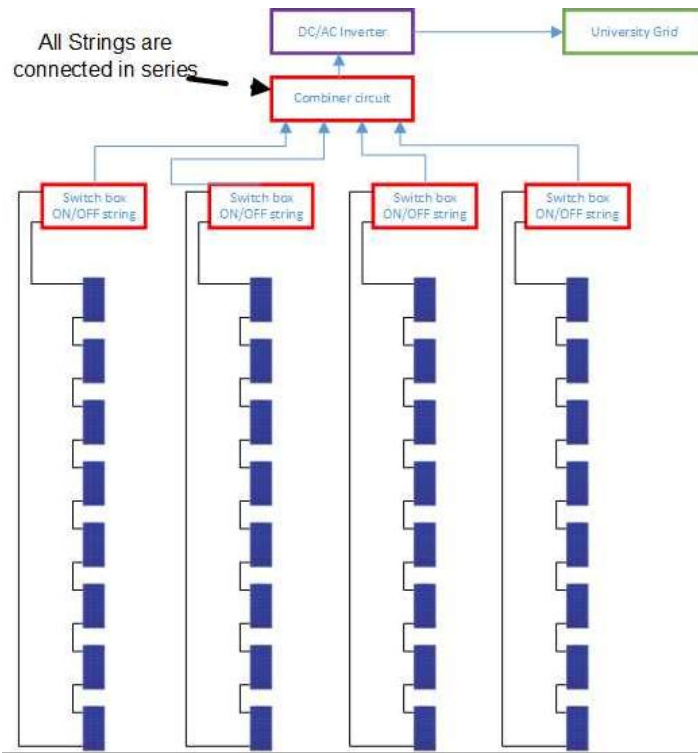
507 The ANN network performed to a higher accuracy in partial shading conditions as compared to  
 508 overcast conditions. However, the overall accuracy of both systems was over 95% with a  
 509 difference of 1.4% in terms of accuracy, between the two networks. The overcast conditions did  
 510 not have a significant impact on the accuracy of the ANN, demonstrating the robustness of the  
 511 system. It is important to note that although the sample data from both conditions was the same,  
 512 the actual content of the data varied (the solar irradiance was much lower for overcast conditions  
 513 as compared to partial shading). The developed ANN was able to handle this variance in the input  
 514 data, through its training and validation, testifying its effectiveness through the overall detection  
 515 accuracy for both conditions, as shown in the respective confusion matrices, Figures 18 and 21.

516 **4.3. ANN results with different PV system**

517 To validate the detection accuracy of the developed ANN, the network was tested with a different  
 518 PV plant (refer to Figure 22). The plant contained four PV strings, each consisting of 8 PV panels  
 519 with all strings connected in series. The switches on the inverter allowed the switching on-off of a  
 520 whole string. However, only one string was to be switched off at any given time representing 8  
 521 faults. If two strings were taken off-line, the occurred faults would equal 16, this was not within  
 522 the scope of this research. The total capacity of the examined PV system is equal to 4.16 kW.



(a)



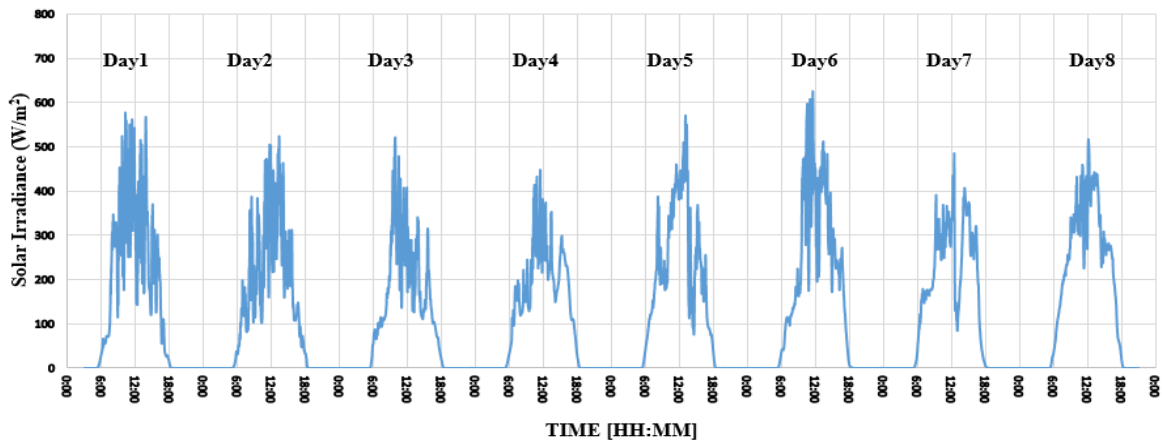
(b)

**Figure 22.** (a) Actual setup of PV system, (b) PV system schematic for test case study

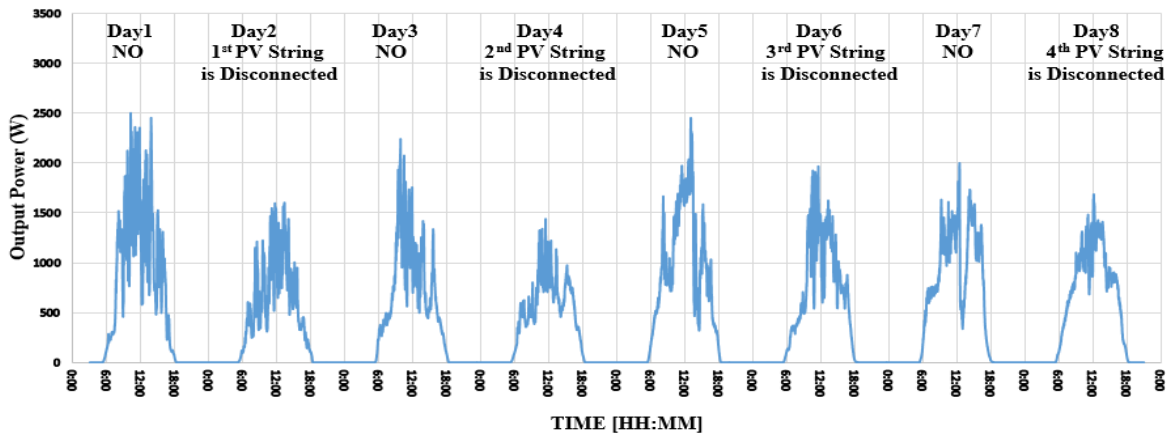
523 The test procedure involved inducing 8-faults by switching off a complete string, followed by  
 524 normal operation for the next day, refer to Table 3. The solar irradiance and total power for the  
 525 duration of the testing period is represented in Figure 23; comprising of overcast and partial  
 526 shading conditions.

**Table 3.** Methodology for test case

No. Days	Condition Applied
1	NO
2	1st string is disconnected
3	NO
4	2nd string is disconnected
5	NO
6	3rd string is disconnected
7	NO
8	4th string is disconnected



(a)



(b)

**Figure 23.** (a) Solar irradiance, (b) Output power for test case

527 Figure 24 illustrates the overall detection accuracy of the developed ANN for the test case PV  
528 system shown in Figure 22. Before extracting any conclusions on the accuracy of the ANN, based  
529 on the comparison of the two PV systems, key factors need to be considered. The first important  
530 factor is the significant variation in the total power capacity of the two systems (2.2 kW and 4.16  
531 kW). Achieving an accuracy of over 96% for both PV systems, the ANN has shown it is highly  
532 adaptable to various capacity of PV systems. Another critical factor was the substantial difference  
533 of the sample data for training the ANN. The first PV system provided the ANN with ‘rich’ training  
534 data consisting of every hour of the day, for a duration of 10-weeks. Whereas, the latter system  
535 reported in this sub-section decreased the amount of training data to 8-days. Nevertheless, the  
536 overall detection accuracy of the ANN for both PV systems boasted results of over 96%. This  
537 again testifies to the reliability, adaptability and successful implementation of our proposed ANN.

538 In order to validate the latter ANN network, an evaluation of the total detection accuracy was  
539 carried out every two days interval. The reason for the selection of ‘two-day’ intervals was due to  
540 the first day consisting of normal operation “NO” followed by 8-faulty “F8” (induced faults by  
541 switching of a whole string, refer to, Figure 22(b)) for the second day. The ANN network original  
542 MATLAB code is shown in Appendix A.

543 Hence, the results of the ANN network during the first two days including NO “as in first day”  
544 and 8-faulty PV modules “as in the second day” is shown in Figure 24(a). The attained detection  
545 accuracy is equal to 97.4%. The main factor that the detection accuracy slightly dropped during 8-  
546 faulty “F8” mode, was due to 26 samples being incorrectly classified as either 9-faulty or 10-faulty  
547 PV modules, resulting in a 2.1% decrease in accuracy.

548 The following 2-days (days 3-4), shown in Figure 24(b), experienced an increase in the overall  
549 detection accuracy of the ANN at 98.0%. The improvement in the overall accuracy was due to the  
550 ANN misclassifying 16 samples as 9-faulty or 10-faulty, when the actual fault induced was 8-  
551 faulty “F8” relating to an error of 1.3%.

552 In contrast to the above pattern of gradual increase in the overall detection accuracy as the week  
553 progressed, day 5 and 6, shown in Figure 24(c) showed signs of deterioration in the over accuracy  
554 of the ANN (96.6%). A total of 43 samples were incorrectly classified as 9-faulty or 10-faulty  
555 instead of 8-faulty.

556 The last two days (days 7 and 8), shown in Figure 24(d) indicated towards an improvement in the  
557 overall detection accuracy of the network, with a total accuracy of an impressive 98.1%. Similarly,  
558 to the first two days (days 3 and 4), 15 samples were incorrectly classified as either 9-faulty or 10-  
559 faulty PV modules, whereas the induced fault consisted of 8-faulty, this led to the reduction in the  
560 overall accuracy by about 0.9%.

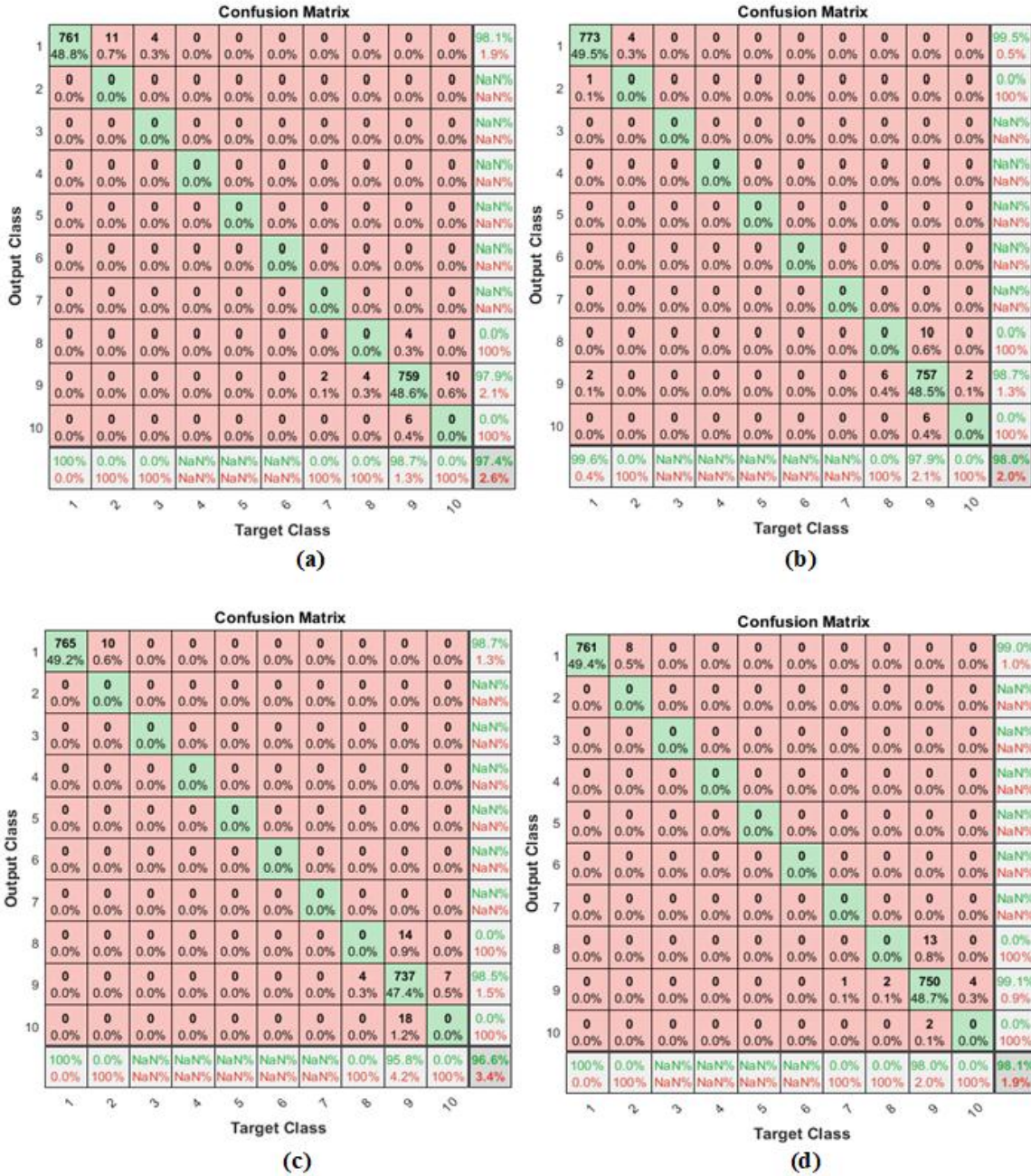


**Figure 24.** Classification Confusion Matrices for the ANN based on the test case PV system shown previously in Figure 22. **(a)** Accuracy is 97.4% for the first 2 days, **(b)** 98.0% for days 3 and 4, **(c)** 96.6% for days 5 and 6, **(d)** 98.1% for the last 2 days (day 7 and 8)

561 **5. Comparative Study**

562 This section evaluates and compares the new research outcomes [24, and 26-28] in the field of  
 563 ANN PV fault detection systems against our proposed methodology. A comprehensive evaluation  
 564 of the methodologies is summarized in Table 4.

565 As illustrated, all recent ANN-based PV fault detection systems require a large number of input  
 566 parameters for the ANN network to operate; hence, the algorithm becomes more complex in terms  
 567 of the practicality as well as the required historical data for the ANN training/validation process.

568 However, in this article, the proposed ANN network only requires two input parameters in order  
 569 to activate, namely the irradiance and the output power, while there is no need of any other PV  
 570 parameters such as the  $V_{mpp}$  and  $I_{mpp}$  as appear in all other recent algorithms [24, and 26-28].

571 The other advantage of our proposed algorithm is that the ambient temperature has not been  
 572 included in the ANN architecture. Hence, temperature sensors are no longer required in the PV  
 573 installation, as this is required by the algorithms proposed by [24] and [28].

574 According to our method, the ANN detection accuracy is ranging from 96.5%~98.1% in normal  
 575 operation (NO) and partial shading conditions, respectively. So far, the obtained PV fault detection  
 576 accuracy is considered the highest, as illustrated in Table 4.

577 Based on the examined PV installations shown earlier in Figures 2(a) and 22(a), the data  
 578 acquisition of the produced power occur at the DC side after the MPPT unit is placed. This place  
 579 of sampling data can generally not be taken for granted to be expandable to other PV systems since  
 580 not many commercial inverters offer this signal to be extracted. Taking this restraint into  
 581 consideration, this becomes the main limitation of the proposed model developed in this article.

**Table 4.** Comparitive study of recent ANN-based PV fault detection algorithms [24, and 26-28] and our proposed method

Ref.	Year	Number of examined PV modules “connected in series”	ANN Methodology – required input parameters							ANN detection accuracy (%)		
			G	T <sub>amb</sub>	P	I <sub>sc</sub>	V <sub>oc</sub>	I <sub>mpp</sub>	V <sub>mpp</sub>	No. of required parameters	Normal Operation	Partial Shading
[24]	2016	Four 25% each setp	✓	✓	✓	✗	✗	✓	✓	5	90.3~97	max:90.3
[26]	2017	Up to Five 20% each step	✓	✗	✗	✓	✓	✓	✓	5	96.5	n/a
[27]	2018	Five 20% each step	✗	✗	✓	✓	✓	✓	✓	4	97.1~95.3	87.3~92.1
[28]	2019	Up to four 25% each step	✓	✓	✓	✗	✗	✓	✓	5	87.4~98.5	max: 66.45
Our proposed algorithm	2020	Ten 10% each step	✓	✗	✓	✗	✗	✗	✗	2	98.1%	96.5%

## 582        6. Conclusion

583        In this article, we have presented four different methodologies to detect PV faults based on two  
584        inputs parameters; solar irradiance and output power. It was found that the ANN accuracy  
585        increased up to 98.1% based on the implementation of the fourth methodology consisting of data  
586        normalisation as well as mapping of solar irradiance against output PV power. Hence, this  
587        methodology has been tested on two different PV installations, with significantly different  
588        electrical parameters.

589        Results show that the developed ANN network accurately detected PV faults in the range of 96.5-  
590        98.1% during normal operational mode, where no shading/overcast is present. Whereas, during  
591        partial shading conditions, the minimum ANN network accuracy deteriorated to was 96.2%. This  
592        outcome is based on the evaluation of our ANN on two differing PV installations, demonstrating  
593        the robustness and adaptability of the proposed network architecture.

594        In future, it is intended to enhance the accuracy of the developed ANN network through the  
595        evaluation of different methodologies comprising of different ANN input parameters as well as  
596        using deep learning methods to enhance the capabilities of the ANN neurons during  
597        training/validation.

## 598        7. References

- 599        1. Di Piazza, M. C., Viola, F., & Vitale, G. (2018). Evaluation of ground currents in a PV system with high  
600        frequency modeling. *International Journal of Renewable Energy Research*, 8(3), 1770-1778.
- 601        2. Dhimish, M., Holmes, V., Mehrdadi, B., Dales, M., Chong, B., & Zhang, L. (2017). Seven indicators variations  
602        for multiple PV array configurations under partial shading and faulty PV conditions. *Renewable Energy*, 113,  
603        438-460.
- 604        3. Mansouri, M., Hajji, M., Trabelsi, M., Harkat, M. F., Al-khazraji, A., Livera, A., ... & Nounou, M. (2018). An  
605        effective statistical fault detection technique for grid connected photovoltaic systems based on an improved  
606        generalized likelihood ratio test. *Energy*, 159, 842-856.
- 607        4. Dhimish, M., & Holmes, V. (2016). Fault detection algorithm for grid-connected photovoltaic plants. *Solar*  
608        *Energy*, 137, 236-245.
- 609        5. Tadj, M., Benmouiza, K., Cheknane, A., & Silvestre, S. (2014). Improving the performance of PV systems by  
610        faults detection using GISTEL approach. *Energy conversion and management*, 80, 298-304.
- 611        6. Mellit, A., & Pavan, A. M. (2010). A 24-h forecast of solar irradiance using artificial neural network:  
612        Application for performance prediction of a grid-connected PV plant at Trieste, Italy. *Solar Energy*, 84(5), 807-  
613        821.
- 614        7. Takashima, T., Yamaguchi, J., Otani, K., Oozeki, T., Kato, K., & Ishida, M. (2009). Experimental studies of  
615        fault location in PV module strings. *Solar Energy Materials and Solar Cells*, 93(6-7), 1079-1082.
- 616        8. Dhimish, M., Mather, P., & Holmes, V. (2018). Evaluating power loss and performance ratio of hot-spotted  
617        photovoltaic modules. *IEEE Transactions on Electron Devices*, 65(12), 5419-5427.
- 618        9. L. Schirone, F.P. Califano, M. Pastena Fault detection in a photovoltaic plant by time domain reflectometry  
619        Prog. Photovolt. Res. App, 2 (1994), pp. 35-44.

- 620 10. S. Silvestre, M.A. da Silva, A. Chouder, D. Guasch, E. Karatepe New procedure for fault detection in grid  
621 connected PV systems based on the evaluation of current and voltage indicators *Energy Convers. Manag.*, 86  
622 (2014), pp. 241-249.
- 623 11. Li, X., Wen, H., Hu, Y., & Jiang, L. (2019). Drift-free current sensorless MPPT algorithm in photovoltaic  
624 systems. *Solar Energy*, 177, 118-126.
- 625 12. W. Yuchuan, L. Qinli, S. Yaqin Application of BP neural network fault diagnosis in solar Photovoltaic System  
626 Proceedings of the IEEE International Conference on Mechatronics and Automation, Changchun, China (2009),  
627 pp. 9-12
- 628 13. W.T. Miller III, F.H. Glanz, L.G. Kraft III Cmas: an associative neural network alternative to backpropagation  
629 Proc IEEE, 78 (1990), pp. 1561-1567
- 630 14. Ashok, V., Yadav, A., & Naik, V. K. (2019). Fault Detection and Classification of Multi-location and Evolving  
631 Faults in Double-Circuit Transmission Line Using ANN. In *Soft Computing in Data Analytics* (pp. 307-317).  
632 Springer, Singapore.
- 633 15. Pan, T., Chen, J., Zhou, Z., Wang, C., & He, S. (2019). A Novel Deep Learning Network via Multi-Scale Inner  
634 Product with Locally Connected Feature Extraction for Intelligent Fault Detection. *IEEE Transactions on*  
635 *Industrial Informatics*.
- 636 16. Belaout, A., Krim, F., Mellit, A., Talbi, B., & Arabi, A. (2018). Multiclass adaptive neuro-fuzzy classifier and  
637 feature selection techniques for photovoltaic array fault detection and classification. *Renewable energy*, 127,  
638 548-558.
- 639 17. Belaout, A., Krim, F., Mellit, A., Talbi, B., & Arabi, A. (2018). Multiclass adaptive neuro-fuzzy classifier and  
640 feature selection techniques for photovoltaic array fault detection and classification. *Renewable energy*, 127,  
641 548-558.
- 642 18. Malik, H., & Yadav, A. (2018). EMD and ANN based intelligent model for bearing fault diagnosis. *Journal of*  
643 *Intelligent & Fuzzy Systems*, (Preprint), 1-12.
- 644 19. Javed, W., Chen, D., Farrag, M. E., & Xu, Y. (2019). System Configuration, Fault Detection, Location, Isolation  
645 and Restoration: A Review on LVDC Microgrid Protections. *Energies*, 12(6), 1001.
- 646 20. A. Lapedes, R. Farber Nonlinear signal processing using neural networks (1987)
- 647 21. Mellit, A., Sağlam, S., & Kalogirou, S. A. (2013). Artificial neural network-based model for estimating the  
648 produced power of a photovoltaic module. *Renewable Energy*, 60, 71-78.
- 649 22. Polo, F. A. O., Bermejo, J. F., Fernández, J. F. G., & Márquez, A. C. (2015). Failure mode prediction and  
650 energy forecasting of PV plants to assist dynamic maintenance tasks by ANN based models. *Renewable Energy*,  
651 81, 227-238.
- 652 23. Yagi, Y., Kishi, H., Hagihara, R., Tanaka, T., Kozuma, S., Ishida, T., ... & Kiyama, S. (2003). Diagnostic  
653 technology and an expert system for photovoltaic systems using the learning method. *Solar energy materials*  
654 *and solar cells*, 75(3), 655-663.
- 655 24. Chine, W., Mellit, A., Lughy, V., Malek, A., Sulligoi, G., & Pavan, A. M. (2016). A novel fault diagnosis  
656 technique for photovoltaic systems based on artificial neural networks. *Renewable Energy*, 90, 501-512.
- 657 25. Yuchuan Wu, Qinli Lan and Yaqin Sun, "Application of BP neural network fault diagnosis in solar photovoltaic  
658 system," 2009 International Conference on Mechatronics and Automation, Changchun, 2009, pp. 2581-2585.
- 659 26. Karmacharya, I. M., & Gokaraju, R. (2017). Fault location in ungrounded photovoltaic system using wavelets  
660 and ANN. *IEEE Transactions on Power Delivery*, 33(2), 549-559.
- 661 27. Dhimish, M., Holmes, V., Mehrdadi, B., & Dales, M. (2018). Comparing Mamdani Sugeno fuzzy logic and  
662 RBF ANN network for PV fault detection. *Renewable energy*, 117, 257-274.
- 663 28. Fadhel, S., Delpha, C., Diallo, D., Bahri, I., Migan, A., Trabelsi, M., & Mimouni, M. F. (2019). PV shading  
664 fault detection and classification based on IV curve using principal component analysis: Application to isolated  
665 PV system. *Solar Energy*, 179, 1-10.



666 **Appendix A**

667 ANN Matlab Code:

668 **function** [y1] = myNeuralNetworkFunction(x1)

669 **% Input 1**

670 x1\_step1.xoffset = [0;0];

671 x1\_step1.gain = [2;2];

672 x1\_step1.ymin = -1;

673 **% Layer 1**

674 **b1** = [-0.53379789162008717263;-5.6867963876778855337;10.177896012639834566;-2.5991370178094546084;-

675 0.95996065238647498852;2.9461760878212293058;4.3468884838846104657;-1.6827716763193365512;-

676 15.784457032110500663;18.01460876010765233];

677 **IW1\_1** = [10.739580122585271837 -11.159248213784534798;2.5403215144122435198 -

678 0.56388784665404756424;-15.530906692487940646 25.724533995852432611;2.6108726483375148675

679 2.8644466106623927004;2.3492627965250321154 -3.9135393841679908533;2.5621241841492614633

680 1.3108436436418966498;-18.156042599742011845 22.592529645218835554;-2.2026222558534906959

681 4.5796412164194322258;10.73037657323408034 -26.46367903771555774;-4.6700671639881869979

682 22.673036080767015932];

683 **% Layer 2**

684 **b2** = [-0.60795246307066741487;0.52920177750850172504;0.87317087958293260197;-

685 0.77428730832701464504;0.80856340475453847283;-0.98776905950334870088;-

686 0.038084773428153848029;0.17631768142364898089;0.1177441519341838605;-1.2286308806154839779];

687

688 **LW2\_1** = [-16.218127732052877832 -0.61842039136869231264 13.65432479360931417

689 0.0279526869588864052 -1.5457829250363672724 -4.5249730228320954595 29.031811827208226617

690 1.3545922631578695139 -7.4451922992102366194 2.1032270854732173504;-1.8610677877454995244 -

691 0.13584261850222981161 14.599061786278145547 0.98142879231714974519 0.023068305715024127467

692 1.2729092739892586827 17.352259289313366253 -1.7969598569705769187 -7.5890283129856896949

693 5.3777628244524660062;0.01769050858020889197 -1.7872590063111608583 14.453052562066568854 -

694 0.28584189135600646114 -2.2943096899107273678 4.6075393554886687753 2.5732414558365808155 -

695 1.3164653264959451651 -9.2113122319186704345 3.9165651867640507433;0.78870635459690852098

696 0.4565538810872159372 15.726589320682379025 1.2188914303559659214 1.5572518953867149349 -

697 0.74512350082267531093 -12.537359667453197076 0.55369386754372895698 -8.5220919780286497058

698 3.4338668969512400331;2.0317783279326593338 -1.1142040895525726629 0.31670104901807094588

699 0.9784865679835351715 0.76022477810981570201 3.7280444386583488914 -9.8244365967376374726

700 0.52810244259625593877 -11.604561582830564603 3.3371779646911083894;1.7526128243198901835

701 0.18517512931874907656 -15.506889259234823086 0.96516150852280624406 0.37972493906172594125 -

702 1.1950923243193563028 -5.2382773533629025664 0.77967472280614491531 -11.860434415464807145

703 5.1071998684124046974;2.1381733507637172842 0.056596023834588657375 -13.298494169561720923

704 0.11021173484657678654 1.2536020059998913556 1.7661104686248074724 -5.336103540167647985

705 0.23036465741826600562 3.3863911471888354932 8.9226575295582417624;3.6723972390395536181

706 0.87284720834851448057 -8.4578343073060278101 -0.044134247790334736605 0.37388197719519100648 -

707 1.0196077545498973826 -5.8551819327672580684 -0.11479275509819439338 17.324612120669645066

708 6.7927117492973421164;6.6441975543224023326 0.44978145240560007956 -8.0408855433529229373 -

709 0.81189573510752477414 0.7060671169563150773 1.493396637034419383 -5.7368690002926161497 -

710 0.87186633673562252689 16.908781753661273228 -9.5834534191820850424;3.0982763799864270204

711 0.49939749005411848692 -8.9893465264005989468 0.36043960291007642871 0.22646282549337756751 -

712 4.3925487668578648837 -5.6103623569920149095 0.51747719198805008922 18.039904522133820564 -

713 27.296588790470323715];

```

714 % ===== SIMULATION =====
715 Q = size(x1,1); % samples

716 x1 = x1'; % Input 1
717 xp1 = mapminmax_apply(x1,x1_step1);

718 a1 = tansig_apply(repmat(b1,1,Q) + IW1_1*xp1); % Layer 1

719 a2 = softmax_apply(repmat(b2,1,Q) + LW2_1*a1); % Layer 2

720 y1 = a2; % Output 1
721 y1 = y1';
722 end

723 function y = mapminmax_apply(x,settings) % Map Minimum and Maximum Input Processing Function
724 y = bsxfun(@minus,x,settings.xoffset);
725 y = bsxfun(@times,y,settings.gain);
726 y = bsxfun(@plus,y,settings.ymin);
727 end

728 function a = softmax_apply(n,~) % Competitive Soft Transfer Function
729 if isa(n,'gpuArray')
730     a = iSoftmaxApplyGPU(n);
731 else
732     a = iSoftmaxApplyCPU(n);
733 end
734 end

735 function a = iSoftmaxApplyCPU(n)
736 nmax = max(n,[],1);
737 n = bsxfun(@minus,n,nmax);
738 numerator = exp(n);
739 denominator = sum(numerator,1);
740 denominator(denominator == 0) = 1;
741 a = bsxfun(@rdivide,numerator,denominator);
742 end

743 function a = iSoftmaxApplyGPU(n)
744 nmax = max(n,[],1);
745 numerator = arrayfun(@iSoftmaxApplyGPUHelper1,n,nmax);
746 denominator = sum(numerator,1);
747 a = arrayfun(@iSoftmaxApplyGPUHelper2,numerator,denominator);
748 end
749 function numerator = iSoftmaxApplyGPUHelper1(n,nmax)
750 numerator = exp(n - nmax);
751 end
752 function a = iSoftmaxApplyGPUHelper2(numerator,denominator)
753 if (denominator == 0)
754     a = numerator;
755 else
756     a = numerator ./ denominator;
757 end
758 end

759 function a = tansig_apply(n,~) % Sigmoid Symmetric Transfer Function
760 a = 2 ./ (1 + exp(-2*n)) - 1;
761 end

```